Flow and transport characteristics at an Epinephelus guttatus (red hind grouper) spawning aggregation site in St...

Article *in* Ecological Modelling · September 2011

DOI: 10.1016/j.ecolmodel.2011.05.031

CITATIONS
15

READS
100

3 authors:

Laurent Cherubin
Florida Atlantic University
40 PUBLICATIONS **1,006** CITATIONS
SEE PROFILE

Richard S Nemeth
University of the Virgin Islands
82 PUBLICATIONS **1,631** CITATIONS
SEE PROFILE

Nasseer Idrisi
The American University of Iraq, Sulaimani
19 PUBLICATIONS **364** CITATIONS
SEE PROFILE

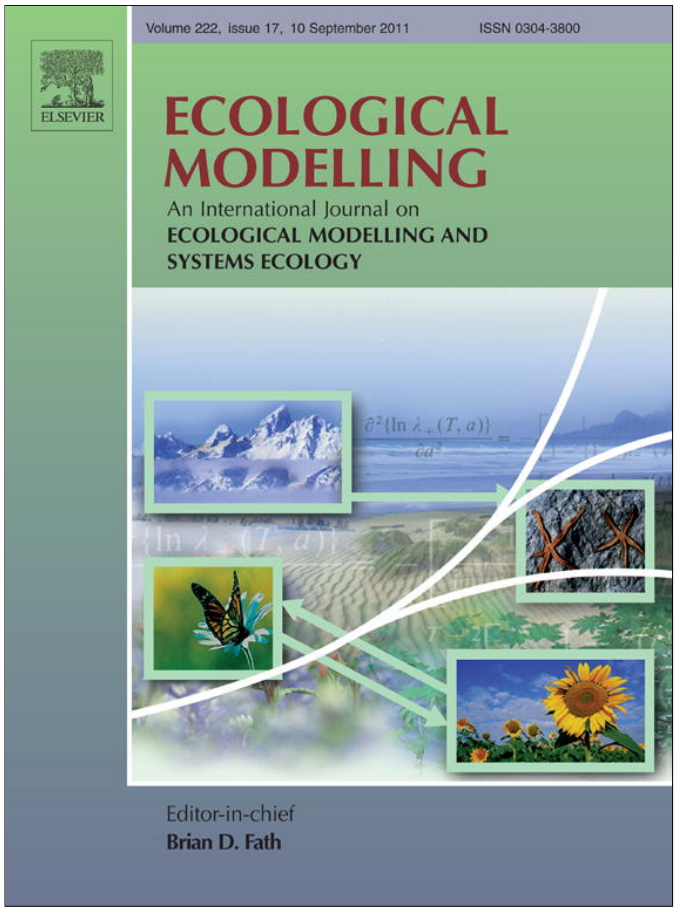

Ecological Modelling 222 (2011) 3132–3148

Contents lists available at ScienceDirect

Ecological Modelling

journal homepage: www.elsevier.com/locate/ecolmodel

Flow and transport characteristics at an *Epinephelus guttatus* (red hind grouper) spawning aggregation site in St. Thomas (US Virgin Islands)

L.M. Cherubin[a,*], R.S. Nemeth[b], N. Idrisi[b]

[a] University of Miami, Rosenstiel School of marine and Atmospheric Science, Division of Meteorology and Physical Oceanography, 4600 Rickenbacker Causeway, Miami, FL 33149, USA

[b] University of the Virgin Islands, Center for Marine and Environmental Studies, St. Thomas, U.S. Virgin Islands

ARTICLE INFO

Article history:
Received 6 December 2010
Received in revised form 13 May 2011
Accepted 14 May 2011

Keywords:
Spawning aggregation
Sub-mesoscale
Tide
Shelf break
Modeling
Retention
Epinephelus guttatus (red hind grouper)

ABSTRACT

This study characterizes the flow field at a spawning site located at the shelf break of a Caribbean island for the *Epinephelus guttatus* (red hind grouper) in relation to this species spawning events. In order to understand the oceanographic dynamics targeted by the fishes, current measurements were profiled throughout the water column for almost a year at the spawning site. The characteristics of the flow field and its evolution after spawning were investigated by using a numerical ocean model that resolved the observed tide and simulated the island scale flow where passive, neutrally buoyant virtual particles were released for 10 days to trace the flow pathways.

Observed currents during the spawning period revealed that the flow was vertically sheared, to the south and weakest at the bottom, and to the west or east at the surface. The tidal analysis revealed that the flow at the time of spawning was directed across and on-shelf, although weaker close to the bottom. The model showed that the initial on-shelf transport was counteracted by the bottom flow directed to the shelf break, where virtual particles were entrained by the downwelling flow. A significant percent of particles resided less than two hundred meters deep, in the vicinity of the chlorophyll maximum and returned to the shelf break, close to the release location within 8–10 days. This journey was largely controlled by the timing between downwelling at the spawning site and upwelling further east at the shelf break, which was driven by the coupling between wind and tide induced vertical movements at the shelf break and deeper. The release location, vertical rotation of its flow field, and its transport properties were shown to be relatively resilient to the passage of transient sub-mesoscale eddies as well as to acute mesoscale flow reversals, suggesting that physical retention is maximized in the area surrounding the spawning site.

1. Introduction

The coupling between fish reproductive strategy and ocean dynamics is a determining factor for the success of broadcast spawning strategy (Cowen et al., 2006; Paris and Cowen, 2004; Paris et al., 2007). Adults of many fish species migrate and aggregate in high densities at a specific location and spawn in a synchronized effort at a specific time (Domeier and Colin, 1997). Migrating to form a spawning aggregation is thought to be conditioned by the presence of specific oceanographic features that would enhance the benefit of reproducing under those conditions in space and time (Johannes, 1978; Lobel, 1978; Barlow, 1981; Robertson, 1991).

Grouper spawning aggregations occur when water temperatures are at 25–27 °C, and this temperature range is found throughout the Caribbean regardless of latitude at the depths where grouper typically spawn (Colin, 1992; Nemeth, 2009). Spawning aggregation sites are located usually at shelf breaks between 20 and 50 m depth (Heyman and Kjerfve, 2008; Claro and Lindeman, 2003), occur during the winter months with a peak from January to March depending upon the species (Domeier and Colin, 1997; Heyman and Requena, 2002; Sala et al., 2001; Nemeth, 2005), and spawning activity occurs primarily in the late afternoon hours around sunset (Colin, 1992; Nemeth, 2009). Sadovy-de-Mitcheson et al. (2008) also noted that 90% of documented aggregations throughout the world occur in reef pass channels, promontories, and outer reef slopes.

Spawning by individual species of groupers occurs during specific narrow windows of time (usually 1–3 months), generally centered on a particular lunar phase (Johannes, 1978; Sadovy et al., 1994; Sadovy and Eklund, 1999; Heyman and Kjerfve, 2008). Since lunar periodicity in spawning peak is closely linked to tidal current amplitude and phase, tide may represent an important component

* Corresponding author. Tel.: +1 305 421 4892; fax: +1 305 421 4696.
E-mail address: lcherubin@rsmas.miami.edu (L.M. Cherubin).

0304-3800/$ – see front matter © 2011 Elsevier B.V. All rights reserved.
doi:10.1016/j.ecolmodel.2011.05.031

of the current dynamics at the spawning site. For example, Storlazzi et al. (2006) show in their Fig. 3 the repeated timing of coral spawning with the tide phase. Coral spawning occurs close to slack tide. As spawning occurred over a 4-day period, the tide phase slightly shifted toward the end of the ebb tide as spawning was occurring at the same time everyday. In Belize, Heyman et al. (2005) studied a *Lutjanus cyanopterus* (cubera snapper) spawning aggregation. They found that the tide phase shifted from ebb to flood over a 5-day period, which suggests again that spawning occurs around slack tide, while the phase slightly shifted as in Storlazzi et al.'s (2006) observations. In the Marshall Islands, Colin and Bell (1991) found that tidal cycles had a stronger influence on the timing of spawning of species that spawned during the day than those that spawned in the late afternoon or at sunset. Most of these diurnal spawning species spawned at slack high tide or shortly after, a behavior facilitating off-shore transport of eggs and has been observed for scarid (parrotfishes) and labrid (wrasses) fishes at many other locations (Robertson and Hoffman, 1977; Ross, 1983; Moyer, 1989; Hensley et al., 1994). These studies suggest that tide driven flow field could be selected purposefully.

In addition to the precise timing and specific location of spawning, the effect of bottom topography on the flow field seems to also influence the depth at which the release of gametes will take place. In Belize, at Gladden Spit Reef, multi-species spawning was observed to occur at the shelf edge, inshore and offshore of the shelf drop (Heyman et al., 2005; Heyman and Kjerfve, 2008). At several locations throughout the wider Caribbean such as Belize, Bermuda, Cayman Islands and the US Virgin Islands, serranids that spawn in groups (i.e. *Mycteroperca bonaci, M. venenosa, Epinephelus striatus*) spawn 10–20 m above the bottom in water 40–90 m deep, 8–10 m away from the shelf break and 20–50 meters below the surface (Whaylen et al., 2004; Nemeth et al., 2006; Starr et al., 2007; Heyman and Kjerfve, 2008; Luckhurst, 2010). At some of these same spawning aggregation sites snappers (Lutjanidae) spawn at slightly different locations and depths later in the spring (Heyman and Kjerfve, 2008; Nemeth et al., 2006; Kadison et al., 2006). It seems that the depth of spawning varies with species but also with locations, suggesting a choice based on site-specific environmental conditions.

In a recent study Nemeth et al. (2008) recorded current speed and direction and bottom temperature using a bottom mounted acoustic Nortek Aquadopp current profiler (NAP) during the spawning season at three separate *Epinephelus guttatus* (red hind grouper) spawning aggregation sites located in St. Thomas and St. Croix, USVI, and in Saba, Netherlands Antilles. Even though the distance between the three locations ranged from 60 to 150 km and each spawning site had a different orientation relative to the shelf break, they found that during the week of spawning, the current would carry fertilized eggs and larvae back onto the shelf. In a separate study, Nemeth et al. (2007) also found that the majority of *E. guttatus* within both St. Thomas and St. Croix spawning populations migrated up current to their respective spawning aggregation site. Nemeth et al. (2008) postulated that if eggs and newly hatched larvae drift slowly down current, they may be in the vicinity of adult home ranges at time of settlement. These and other studies also suggested that certain physical features might be consistent across multiple spawning sites, such as the presence of slower cross-shelf currents during the week of spawning (Appeldoorn et al., 1994; Nemeth et al., 2007; Nemeth et al., 2008).

In this study, we investigate the physical processes that are involved during the spawning period at the St. Thomas *E. guttatus* spawning aggregation site in order to describe the physical environment that the eggs and larvae will be exposed to, which is important for predicting their distribution (Johannes, 1978; Barlow, 1981; Doherty et al., 1985; Gladstone, 2007). We attempt to address the following questions in regards to their spawning strategy: what specific oceanographic features are targeted by the fish? How determining is timing and depth of release to the fate of particles released at the spawning site? To address these questions, we focus on the tidal and the subtidal flow properties, driven by the local topography, and its effects on the meoscale and sub-mesoscale flow at the spawning aggregation site. In this paper we analyze the observed flow field and its tidal characteristics at the spawning site in regards to the timing of spawning. We present a numerical model implementation of the flow circulation at the study site, validate the numerical model tidal flow with the in situ measurements, and analyze the Lagrangian flow field in the model by releasing neutrally buoyant, virtual, passive particles.

2. Methods

2.1. Study site and species

In the northern United States Virgin Islands (USVI), *Epinephelus guttatus* form a large spawning aggregation 12 km south of St. Thomas, in 45 m of water and 300 m away from the shelf edge (Fig. 1). The Red Hind Bank is characterized by structurally complex coral reef habitat about 100 m from the shelf edge ranging from 30 to 50 m depth (Armstrong et al., 2006; Nemeth et al., 2007). This site was chosen for ocean current measurements because it is a well known spawning site of *E. guttatus*, which aggregates each year between December and February (Beets and Friedlander, 1999; Nemeth, 2005; Nemeth et al., 2007). Spawning typically peaks on the week of the full moon in January (Shapiro et al., 1993; Nemeth, 2005), with numbers of spawning adults in December and February determined by the timing of the full moon (Nemeth et al., 2007, 2008). During the December 2005 to February 2006 spawning season, the presence of the *E. guttatus* spawning aggregation in St. Thomas was validated by using fish counts conducted by SCUBA along 30 m × 2 m belt transects (Nemeth et al., 2008). Spawning was verified based on changes in the gonado-somatic index (GSI) of female *E. guttatus* during a 6-day period from 3 days before to 2 days after the January 2006 full moon (Nemeth et al., 2008). Peak *E. guttatus* densities occurred 2 days before the full moon and GSI was greatest on the full moon suggesting that spawning occurred during this 3-day period and peaked on the full moon (Nemeth et al., 2008). Based on courtship behaviors, pair spawning is assumed to occur just a few meters above the bottom (Shapiro et al., 1993; Nemeth et al., 2007). Fertilized eggs of *E. guttatus* are 0.97 mm diameter and hatch in 27 d at 26.5 °C, which is within the range of temperature this species spawns throughout the Caribbean including Bermuda (Burnett-Herkes, 1975; Colin et al., 1987; Luckhurst, 1998; Nemeth et al., 2007). Serranidae absorb their yolk 3–4 days after fertilization and therefore must find food and begin feeding or starve (Powell and Tucker, 1982; Colin, 1992; Katajima et al., 1992; Colin et al., 1997; Martínez-Lagos and Gracia-Lopez, 2009). Groupers within the genus *Epinephelus* and *Mycteroperca* complete post-flexion 17–28 days after hatching at which time they become stronger swimmers and have a pelagic larval duration of 36–46 days (mean = 41.5 d) (Powell and Tucker, 1982; Colin, 1992; Katajima et al., 1992; Richards et al., 2006; Martínez-Lagos and Gracia-Lopez, 2009).

2.2. Flow measurements and tidal analysis

Current measurements were collected at the Red Hind Bank (18° 12.20′ N, 65° 0.10′ W) located about 10 km south of St. Thomas within a protected marine conservation district (MCD). A 600 kHz Nortek Aquadopp profiler (NAP) was deployed in February 2005 and recovered early May 2005 (Period 1, P1) and redeployed mid September 2005 until early March 2006 (Period 2, P2). The

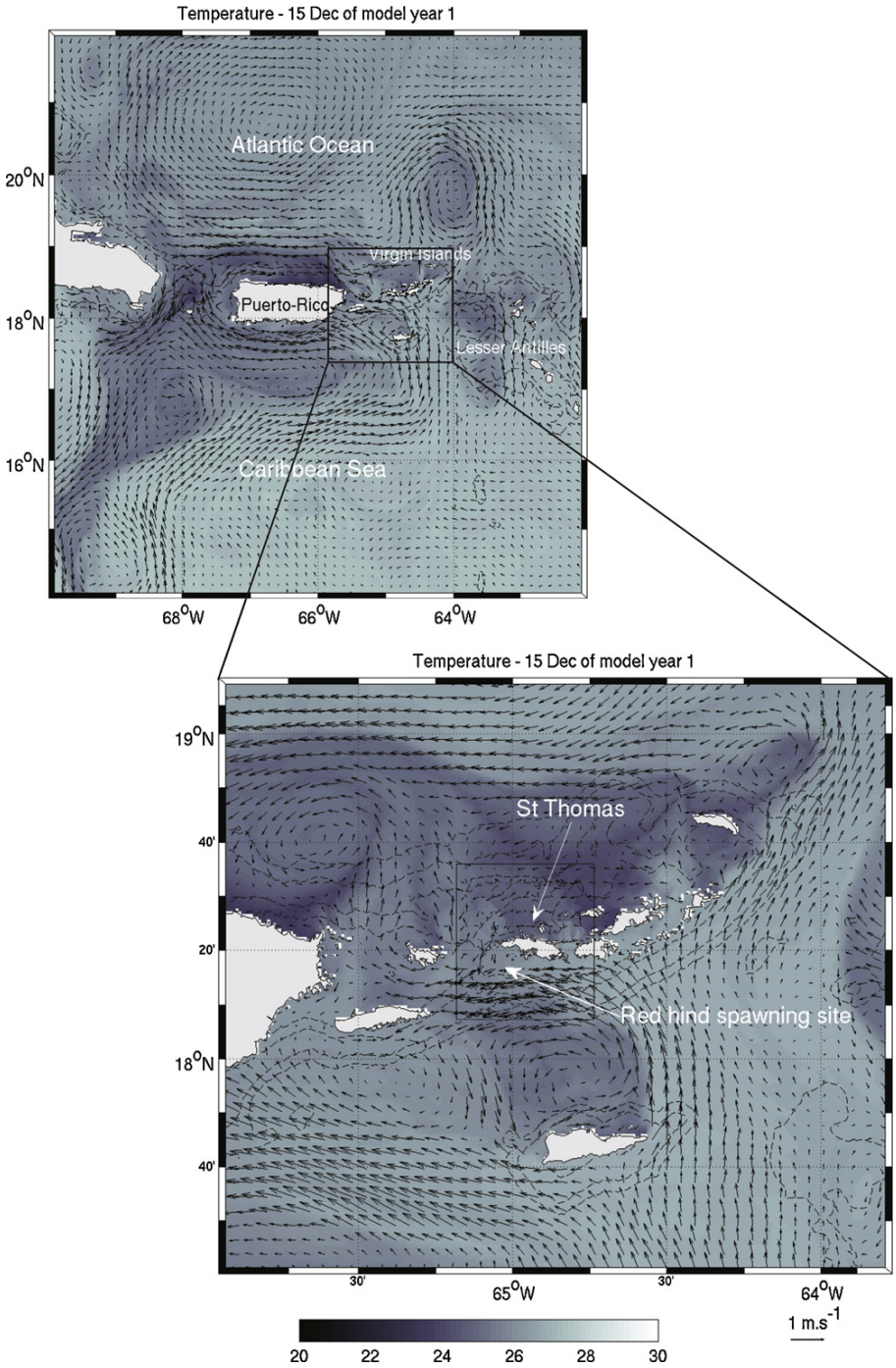

Fig. 1. Snapshots of temperature and currents on model month 15 December showing the area of study and the spawning site. Black squares show each of the sub-domains implemented for the Regional Oceanic Modeling System (ROMS) simulation. Dashed lines in the zoom show the 50, 100, 500 and 1000 m depth contours.

NAP was deployed upward looking near the shelf edge at 41 m depth. Ensemble averages of 4 pings were recorded every 30 min, from which the velocity components were distributed over 45 cells, each 1 m high. NAP data were processed with the Storm software (http://www.nortek-as.com/products/products-2/storm-surge) provided by the manufacturer. The processing was based on signal to noise ratio (SNR) rejection with a 3 dB threshold level, a 70 dB spike rejection level. Being in oligotrophic waters and surrounded by a reef platform, the signal strength of the beams was relatively weak shallower than 15 m although the surface turbulence showed as a relatively strong signal.

In order to illustrate the characteristic contribution of tidal frequencies to the observed horizontal and vertical motion, the vertically averaged power spectra were first determined for each period. Then the part of motion due to coherent baroclinic tidal waves was analyzed, which assumes that amplitude and phase lag were persistent on the time scale of the duration of the measurements (van Aken et al., 2007). Next, the incoherent M2 (principal

lunar semidiurnal) tide was analyzed at a shorter time scale, in which velocity variance, orientation of the tidal ellipse, and vertical structure of the tidal phase and amplitude show variability (van Aken et al., 2007). To determine amplitude and phase of the internal tides, a harmonic analysis of the horizontal velocity measured in the NAP cells was applied. A classical tidal harmonic analysis was performed using the upgraded version by Leffler and Jay (2009) of MATLAB T_TIDE program originally written by Pawlowicz et al. (2002). This analysis was valid for periods of less than one year, accounted for some unresolved constituents using nodal corrections, and computed confidence interval for the analyzed components. Moreover it used MATLAB implementation of iteratively reweighted least squares to reduce the influence of high residual data.

2.3. Ocean model and virtual particle transport

In order to simulate the dispersal of passive particles from the *E. guttatus* spawning site, a very high resolution simulation (330 m) of the northeastern Caribbean Sea was used. This climatological simulation contributed to several studies addressing coral larvae dispersal (Baums et al., 2006), the dynamical influence of the fresh water plumes from the Amazon and Orinoco Rivers (Chérubin and Richardson, 2007), and island wake effect on larval retention in St. Croix, USVI (Chérubin and Paris, unpublished work). This simulation was implemented with the Regional Oceanic Modeling System (ROMS – Shchepetkin and McWilliams, 2004) and constituted three nested domains, one parent and two child domains. The second child domain grid size was 330 m and was centered on St Thomas. The model was forced by oceanographic and atmospheric climatology and by the tide at its boundaries using the Oregon State University TPXO6 (Egbert and Erofeeva, 2002) $0.25^\circ \times 0.25^\circ$ global tide model. Five tidal components M2 (principal lunar, semi diurnal), S2 (principal solar, semi-diurnal), N2 (larger lunar elliptic, semi-diurnal), K2 (luni-solar, semi-diurnal) and, K1 (luni-solar, diurnal) were included. The simulation was shown to reproduce the seasonality of the circulation and of the eddy kinetic energy observed by Lagrangian drifters (Richardson, 2005; Chérubin and Richardson, 2007).

Before using this simulation to study the flow characteristics at the Red Hind Bank, the simulation was implemented with tides corresponding to years 2003–2004. It was used as such in this study since tide characteristics are relatively invariant through the years although the sub-tidal flows could be different. The full moon in model month January 2004 was on the 7th day. At the model *E. guttatus* spawning site, currents and temperature profiles were recorded every 25 min, at a frequency similar as in the observation.

Since peak spawning for *E. guttatus* occurs mostly in January, the Lagrangian experiments were designed to test the changes in dispersal and fate of virtual particles released at the time of spawning around dusk each day of the week of the full moon (Nemeth et al., 2008). One hundred simulated particles were released at the model' spawning site, at every 5 m depth intervals from the surface. Virtual particles were also released at dawn of these days in order to address the influence of timing and at the full moon of model month September in order to estimate the specificity of the month of spawning in comparison to similar periods in the lunar cycle for non-spawning months. In the model's simulation both December and February were characterized by sub-mesoscale and mesoscale flow events, therefore virtual particles were released during both these months at the time of spawning one day before and after the full moon to test the effect of sub-mesoscale and mesoscale flow change on the fate of particles.

To characterize the flow movements in the three-dimensional space, virtual particles were set to be neutrally buoyant. Their trajectories were calculated using the on-line Lagrangian transport module of ROMS. The code uses a fourth-order accurate Adams–Bashford–Moulton predictor-corrector scheme to integrate $d\boldsymbol{x}/dt = \boldsymbol{u}(\boldsymbol{x},t)$ ($\mathbf{x}$ is particle coordinate and $\mathbf{u}$ its velocity vector) over time given the initial release location and the three-dimensional ROMS velocity fields. The right-hand side is estimated through linear interpolation in time and space of the discrete Eulerian fields and a random displacement was added. Two diffusivities ($50\,m^2\,s^{-1}$ and $300\,m^2\,s^{-1}$) were used to parameterize the model unresolved sub-grid scale diffusivity, based on Okubo's diffusion diagram (Okubo, 1971) and to test the trajectories sensitivity to small-scale random dispersion. The effect of the tide was present in the trajectories because the time step of the Lagrangian model was the same as the Eulerian model, 80 s. Virtual particle positions were saved every 6 h, for up to 10 days, 5 days being the time that larval groupers need to swim to search for food (Katajima et al., 1992; Richards et al., 2006; Martínez-Lagos and Gracia-Lopez, 2009).

In order to quantify the dispersion properties of virtual particles we used two metrics. The first one is based on the location of the chlorophyll maximum, which is present between 200 and 50 m in the northern Caribbean Sea (Corredor and Morell, 2001). This region could constitute a feeding zone for the *E. guttatus* larvae. Therefore we estimated the percentage of each release that was at depths shallower than or returned to depths less than 200 m within 8 days as most were entrained down the shelf break. We assume here that currents would carry pre-competent fish larvae off-shelf to feeding zones that would include depths that extend down to 200 m where chlorophyll maxima occur. The second metric is the absolute three-dimensional dispersion tensor

$$D(t, X(0)) = \overline{[x(t) - x(0)][y(t) - y(0)][z(t) - z(0)]}$$

where the overbar denotes an ensemble average over particles released at the same initial position $X(0)$.

3. Results

3.1. Mean and tidal flow field as measured at Red Hind Bank

3.1.1. Mean flow

One of the main sources of seasonality in the eastern Caribbean Sea is the fresh water plume from the Amazon and Orinoco Rivers (Chérubin and Richardson, 2007). The measured flow field was divided according to a "dry season", which encompasses months from January to July and a "wet season", which corresponds to the presence of fresh water from both rivers in the Caribbean Sea and heavy localized rainfall, from August to December. Measurement period P2 (see Section 2.2 for definition of periods) was then divided accordingly into periods September–December 2005 (wet) and January–March 2006 (dry) (Fig. 2).

As expected, the mean flow was slightly faster during the wet season than during the dry season (Fig. 2a–c). During the wet season, a subsurface maximum and minimum were observed due to the presence of fresher water (Fig. 2b). Both dry season measurements were relatively similar and exhibit a strong vertical shear above 15 m (Fig. 2a and c). In general, the bottom flow field was characterized by a minimum velocity at 5 m above the bottom during both the wet and dry seasons. Over both P1 and P2 periods, the maximum vertical shear was $0.08\,m\,s^{-1}$ and the variability range of the flow was similar, about $0.1\,m\,s^{-1}$.

Significant differences were also seen in the mean direction of the flow between the two seasons (Fig. 2d). During the wet season (September–December), the surface flow was to the northwest and veers to the northeast below 11 m, then tended to orient to the south in the last 5 m. During the dry season (January–July), the flow was barotropic in the first 20 m to the west–northwest. It also tended to orient to the south at the bottom in February–May 2005

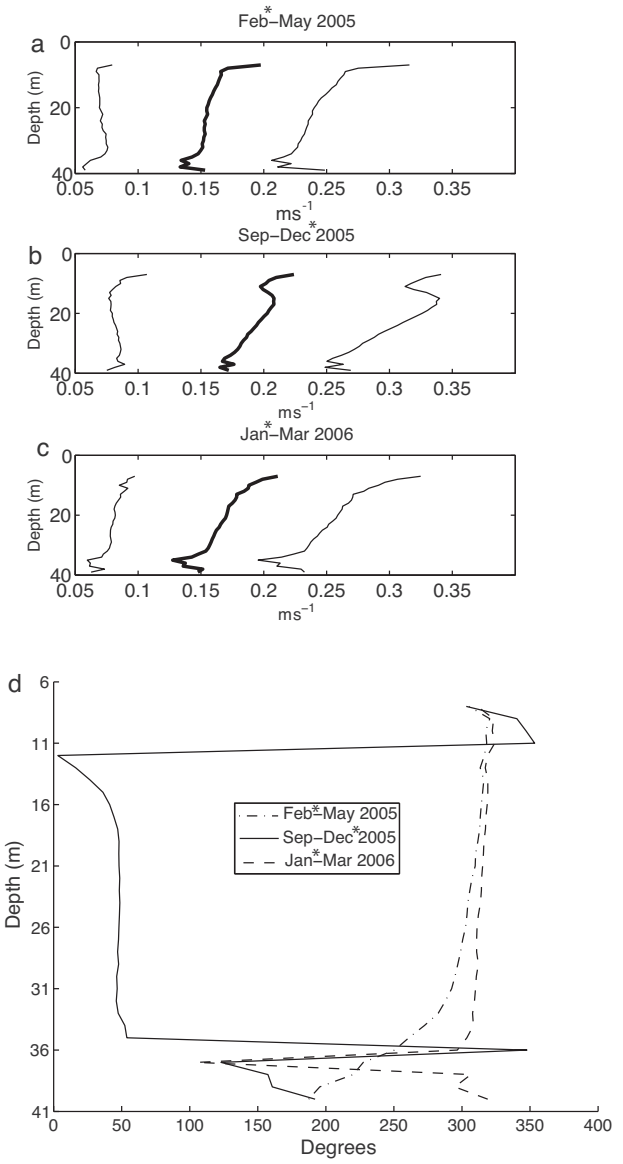

Fig. 2. NAP current vertical mean profile (thick line) and standard deviation (thin lines). (a) Dry season from February to May 2005. (b) Wet season from September to December 2005. (c) Dry season from January to March 2006 and. (d) Seasonal average of the mean direction for periods February–May 2005 (dashed-dotted line), September–December 2005 (solid line) and, January–March 2006 (dashed line). Stars designate the spawning months.

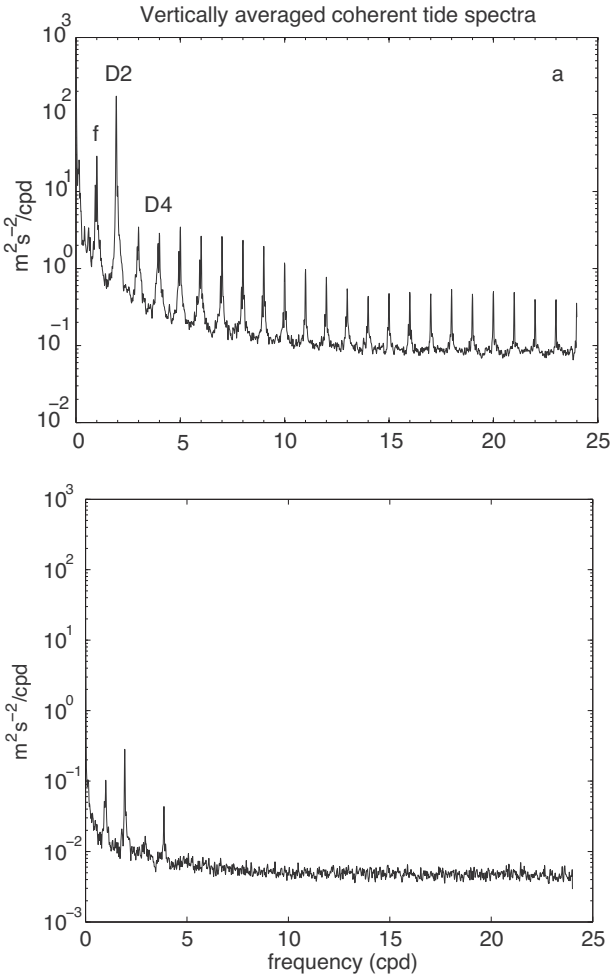

Fig. 3. Vertically averaged coherent tide spectrum for period P2. (a) Horizontal velocity. (b) Vertical velocity. cpd is cycles per day, *f* is the Coriolis frequency, D2 is the M2 (lunar constituent) and S2 (solar constituent) semi-diurnal frequency and D4 its first harmonic.

or to the west in January–March 2006. We will retain here that the vertical shear was associated with an anticyclonic rotation of the flow in the last 5 m if the flow was eastward or cyclonic rotation if the flow was westward.

3.1.2. Tide harmonic analysis and subsequent flow characteristics

3.1.2.1. Spectra. Spectra were determined for successive 44-day periods with a 22-day overlap and averaged subsequently in each NAP cell. These spectra were then averaged over only the first 25 cells in order to prevent the inclusion of data filled with gaps shallower than 25 m. The spectra for the east and north components were summed to obtain information on the frequency distribution of the kinetic energy. The power spectrum for period P2 (which is the longer period of continuous measurements) (Fig. 3a) showed a spectral continuum with a series of spectral spikes in the frequency range up to 24 cpd. The same exact peaks were present during P1 with a slightly different relative amplitude in the high frequencies (>15 cpd – not shown). The dominant spectral peaks were located at the M2 (lunar constituent) and S2 (solar constituent) semi-diurnal (D2) tidal frequencies and their seven first harmonics. The other highest peak in the internal tide band spectrum of the horizontal velocity was observed at the Coriolis frequency *f*. Vertical velocity spectra showed a near-white background spectral continuum, interspersed with very few spectral lines, contrary to the horizontal velocity spectra (Fig. 3b). Only the semi-diurnal tide (D2) and its second harmonic (D4) along with the Coriolis frequency *f* had significant peaks.

3.1.2.2. Coherent tide. The coherent tide characteristics show variations between seasons (Fig. 4). The contribution of coherent harmonic tides to the kinetic energy was larger during the dry season than during the wet season (Fig. 4a–c). The flow was more energetic in the September–December 2005 period and exhibited a surface maximum and a bottom minimum with the largest vertical shear of all seasons (Fig. 4b). For all periods, the M2 tidal constituent is the largest tidal contributor. The contribution of the coherent tide to the total flow kinetic energy (~25–50%) increased with depth

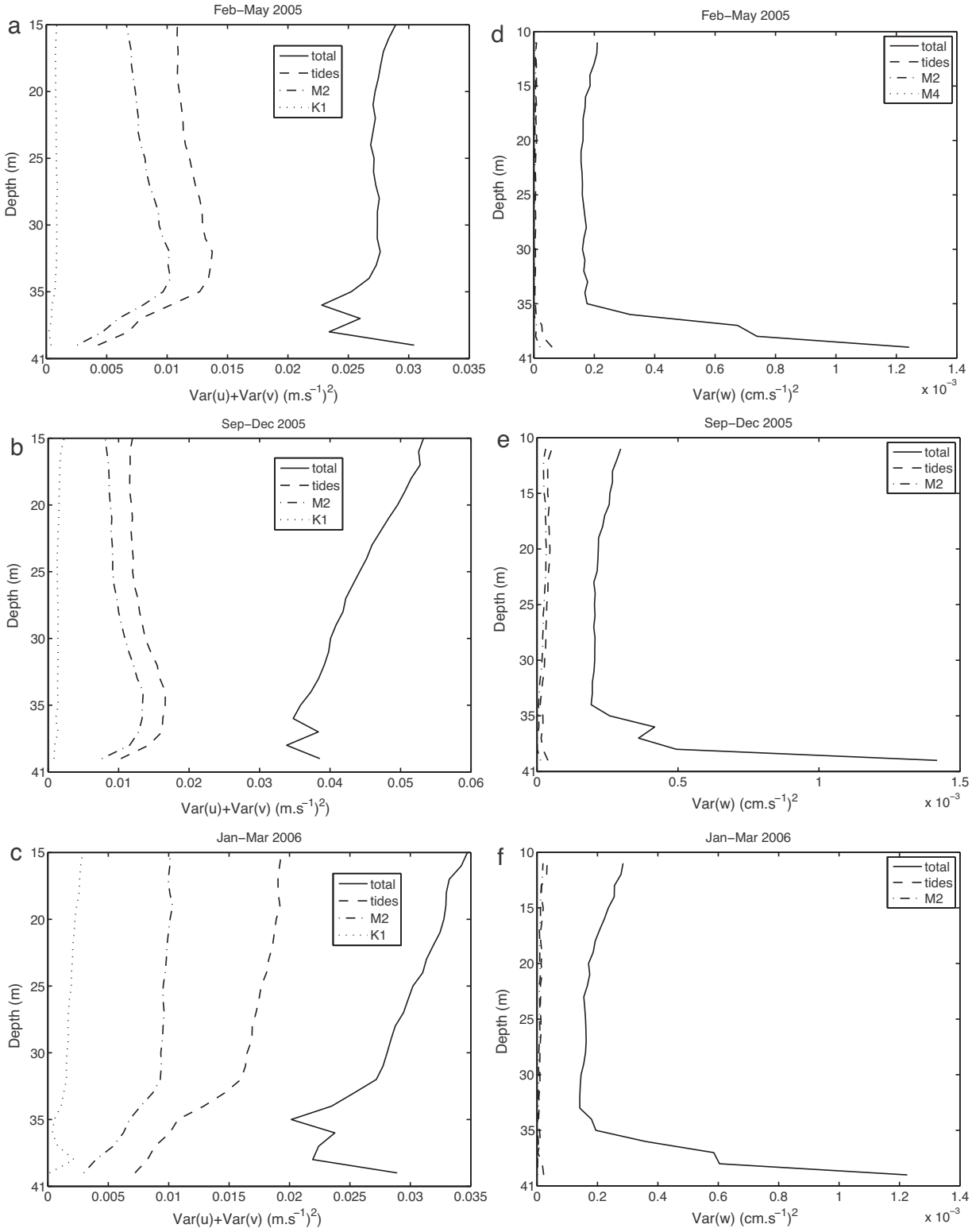

Fig. 4. Variance of the total current (solid line), of the tide (dashed line), of the tidal constituents M2 (dashed dotted line) and K1 (dotted line) for the horizontal velocity (a–c) and for the vertical velocity (d–f) for periods February–May 2005 (a and d); September–December 2005 (b and e); and January–March 2006 (c and f). (g) Vertical velocity tidal phase for periods February–May 2005 (dashed dotted line), September–December 2005 (solid line), and January–March 2006 (dashed line).

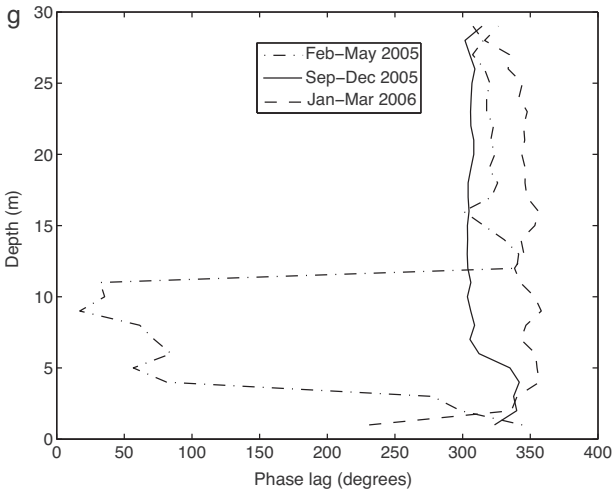

Fig. 4. (*Continued*)

in September–December 2005 contrary to periods February–May 2005 and January–March 2006 although tide contribution was the lowest at the bottom for all periods (Fig. 4a–c). The largest tide driven variance occurred during the period January–March 2006: 69% at 10 m (Fig. 4c). The M2 tidal phase lag of both east and north components was vertically constant (not shown), which indicates that horizontal tidal motions were nearly in phase over the water column.

Seasonal variations were also observed in the tide contribution to the vertical velocity (Fig. 4d–g). The coherent M2 tide accounted for a higher percentage of the variance during the period September–December 2005 (∼15%) than during the two periods in the dry season (∼9% and 4% in February–May 2005 and January–March 2006 respectively – Fig. 4d–f). The contribution of the tide in all periods was minimum at the bottom, maximum in mid water (∼20 m) in February–May 2005 and September–December 2005, whereas it was maximum toward the surface in January–March 2006 (Fig. 4f). In February–May 2005, the phase lag decreased upward in the first 10 m from the bottom by 340° suggesting vertical propagation limited to 10 m above the bottom. During P2 the phase lag of the coherent M2 tide of the vertical velocity was relatively constant vertically (Fig. 4g). It also shows that tide driven vertical motions were not in phase with tide driven horizontal motions. In comparison to the horizontal velocity, the contribution of tide to vertical kinetic energy is not significant. In general most significant tide contribution occurred mostly in the first 35 m from the surface. A significant increase of the vertical velocity variance occurred close to the bottom, in the last five meters, which is not tide driven.

3.1.2.3. Incoherent tide. The previous statistics presented the long-term mean vertical structure of the horizontal and vertical velocity field and of its tidal harmonics. Temporal and vertical variations of the velocity component in the direction of the major axis of the M2 tidal ellipse during three successive days are shown in Fig. 5. The time window was centered on the full moon, which is peak spawning time for *Epinephelus guttatus* (Nemeth et al., 2008). The characteristic direction of the observed tidal ellipse for the 3-day period was defined as the direction in which the total variance of the velocity component for all NAP cells was maximized (van Aken et al., 2007).

The temporal evolution of vertical profiles of the horizontal velocity was analyzed for 3 days of spawning during 23–25 February 2005, full moon on the 24th (Fig. 5a); during 14–16 December 2005, full moon on the 15th (Fig. 5b); during 13–15 January 2006, full moon on the 14th (Fig. 5c); and during 12–14 February 2006, full moon on the 13th (Fig. 5d). For all four months, during the 3 days of spawning, the major axis of the tidal ellipse direction was 160°, 12°, 187° and 180° true north, which is more or less perpendicular to the local shelf. Analysis of flow revealed the barotropicity of the tide yielding synchronous tidal flow reversal in the first 25 m from the bottom, though some cores of stronger or weaker flow were observed during ebb or flood events (Fig. 5). For instance in December 2005 (Fig. 5b), the ebb flow (negative values correspond to southward flow) was stronger in the first 15 meters from the bottom whereas the flood was stronger toward the surface. A similar pattern was also observed in February 2006 (Fig. 5d) (negative values correspond to northward flow). Although there was a general tendency to have stronger flows 10 m and above from the bottom, the flow can be relatively vertically uniform (Fig. 5a). In most cases the barotropicity of the tide regime was more perturbed close to the bottom, in the last 5 m. Finally the variance contributed by the tide at the time of spawning was not significantly higher than the mean observed for the coherent tide.

Regarding the flow characteristics during the time of spawning, *E. guttatus* typically spawn at dusk or after sunset (Shapiro et al., 1993). For all the examples shown here, this time period was not necessarily at slack tide but sometime half way of the half tide cycle (Fig. 5). Based on the direction of the major axis of the tidal ellipse, the flow was always directed toward the shelf.

3.2. Modeled flow and virtual particle transport from spawning site

3.2.1. Comparison of model flow field with observations at spawning site

3.2.1.1. Mean flow. Independently of the season, the model mean flow at the spawning site was swifter than in the observations (Fig. 6). However, the seasonal change associated with the presence of the fresh water plume was also present in the model mean flow. It was swifter during the wet season than during the dry season (Fig. 6a–c). Although surface velocities were two to four times larger in the model than in the observations (Fig. 2a–c), bottom velocities agreed better with the observations and was the area relevant to *E. guttatus* spawning. The near bottom extrema seen in Fig. 2a and c were not present in the model, most likely because of the coarser vertical resolution toward the bottom. The increased

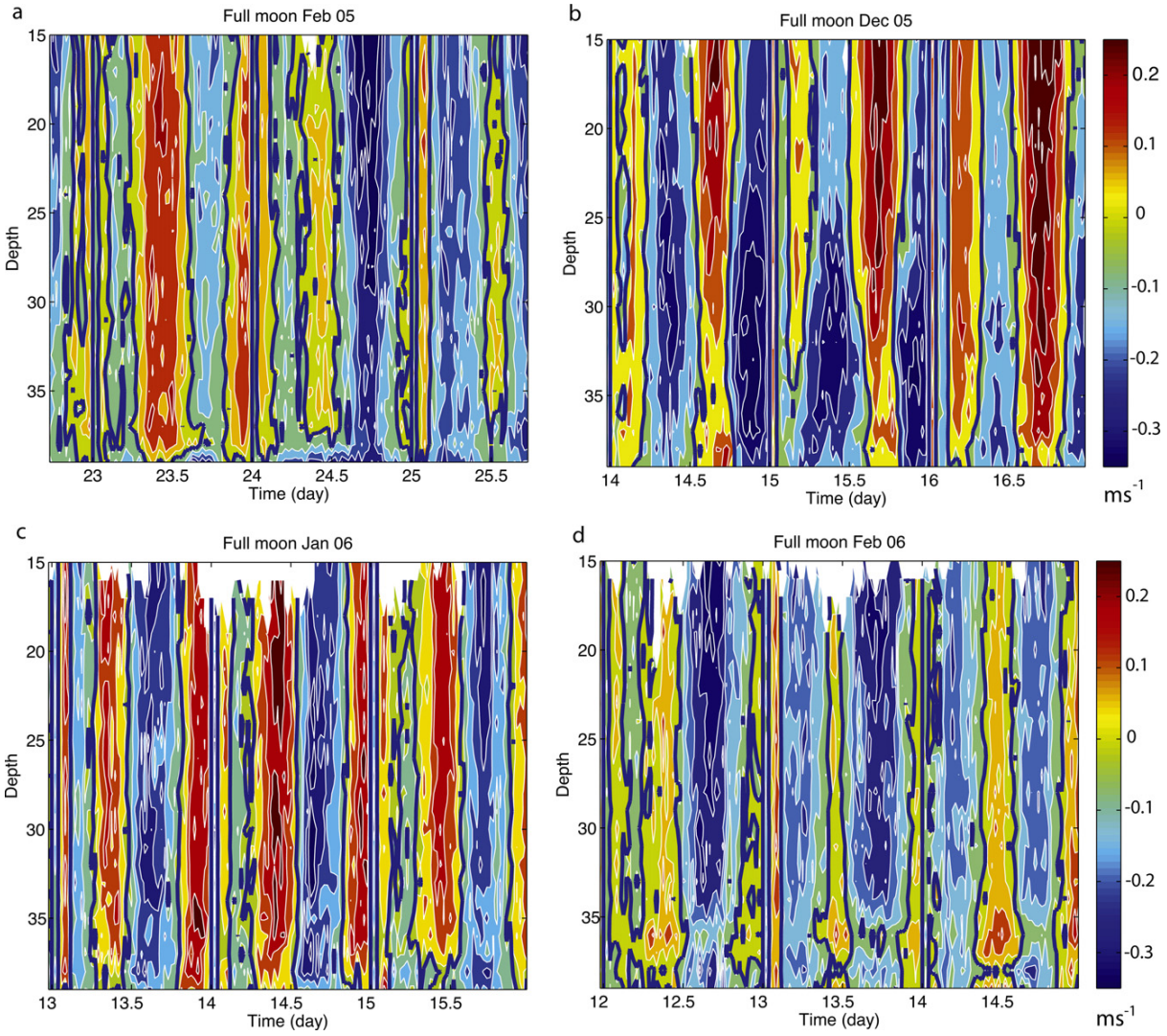

Fig. 5. Three day windows of the velocity along the major axis of the tidal ellipse centered at the full moon of February 2005 (a), December 2005 (b), January 2006 (c), and February 2006 (d). *x*-Axis shows days of the corresponding month and *y*-axis the depth in meters. Blue thick lines show the zero contours ($m\,s^{-1}$). (For interpretation of the references to colour in this figure legend, the reader is referred to the web version of the article.)

surface shear was similar between model and observations for the wet season and for model month January (Fig. 6a and b).

The mean flow directions in model month January (Fig. 6d) agreed well with in situ observations (Fig. 2d). The flow was more to the west at the surface and veered southward toward the bottom. The mean direction in model month February–March was to the east versus to the west in the observations. The mean direction in model months September–December was similar to the model month January unlike the observations (Fig. 2d). Nonetheless, the model reproduced the rotation of the flow to the south with depth.

3.2.1.2. Spectrum and coherent tide characteristics. Simulated current spectra were calculated using a two and half months only time series from model month December to mid February. As the simulation involved running the three domains simultaneously, two months were necessary to complete the time series on a 16-node cluster. Consequently, both the swifter mean flow and the length of the times series yielded the tide variance to be much less than observed (Fig. 7a and b). Nonetheless, similar spectral continuum to the observed values was obtained with less spectral peaks as only five tidal constituents were simulated. The dominant spectral peaks were located at the M2 and S2 semi-diurnal frequencies (D2) and at the Coriolis frequency *f*. The vertical contribution of the coherent tide showed the same variation as the real tide (Fig. 7b). It increased around 25 m deep and its variance was lowest close to the bottom. However, the tide phase changes with depth (Fig. 7c). This difference could be explained by the shorter time series than the observations.

3.2.1.3. Incoherent tide. Because of swifter currents at the model spawning site, the 3-day time series was detrended in order to visualize the tide contribution to the flow on January model full moon 2004. The direction of the major axis of the tidal ellipse was 352°, which yielded a northward cross-shelf flow in late afternoon of January 7th, similar to the observations (Fig. 8). The vertical structure of the tide driven flow in the model was also similar to the observed vertical structure of tide driven flow (Fig. 5).

In summary, although our model time series at a fixed location is relatively short to fully quantify the tide contribution, the model flow field reproduces some of the characteristic features of

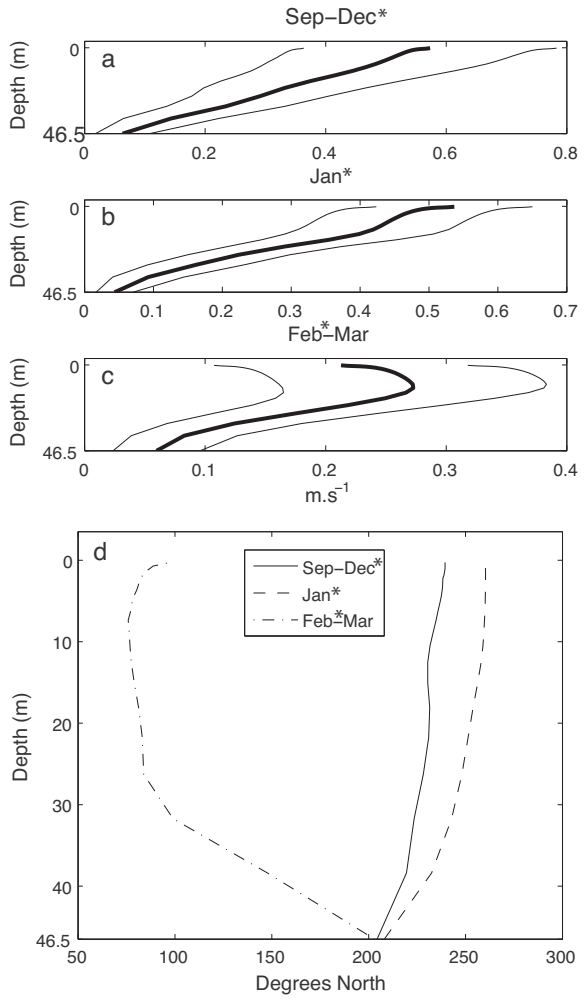

Fig. 6. Model mean profile of the horizontal velocity for periods September–December (a), January (b), and January–February (c). Thick lines show the mean flow and thin lines the standard deviation. (d) Mean flow direction for periods September–December 2005 (solid line), January (dashed line) and for January–March (dashed-dotted line). Stars designate the spawning months.

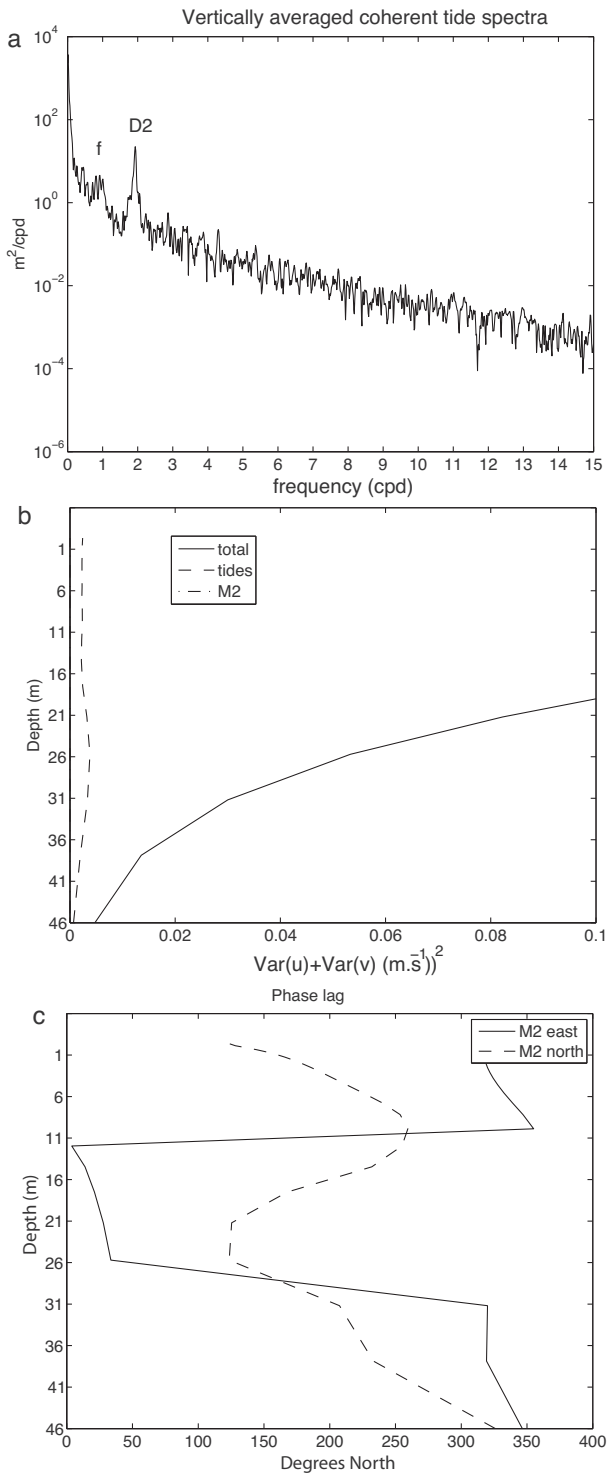

Fig. 7. (a) Vertically averaged spectra of the horizontal velocity for September–December period. (b) Variance of the current (solid line) and of the tidal constituent M2 (dashed line). (c) Phase lag of the tidal constituent M2 east (solid line) and north (dashed line) components.

the observed flow field such as the vertical shear of the mean flow, the relative contribution of the coherent tide to the mean flow and the vertical structure of the incoherent tide. We now build upon the model simulation to study the flow transport characteristics and their subsequent effects on passive neutrally buoyant particles dispersal from the model spawning site.

3.2.2. Lagrangian experiments

3.2.2.1. Particles shallower than 200 m. The percentage of virtual particles that were shallower than 200 m within 8 days varied for each day of release, whereas differences were not significant between depths of release (Fig. 9). On 7 January (full moon) a low percent of particles remained within less than 200 m (Fig. 9a). However, on 8 January release (1 day after full moon) with reduced diffusivity, more than half of the particles were found less than 200 m (Fig. 9b), and on January 9 release (2 days after full moon) at 6:30 am more than 60% were found less than 200 m. All other days of release percent returns have some point where they overlap for the various depths. In September a lower percent remained less than 200 m than in January in general with the highest percent found less than 200 m on 7 September, 3 days before the full

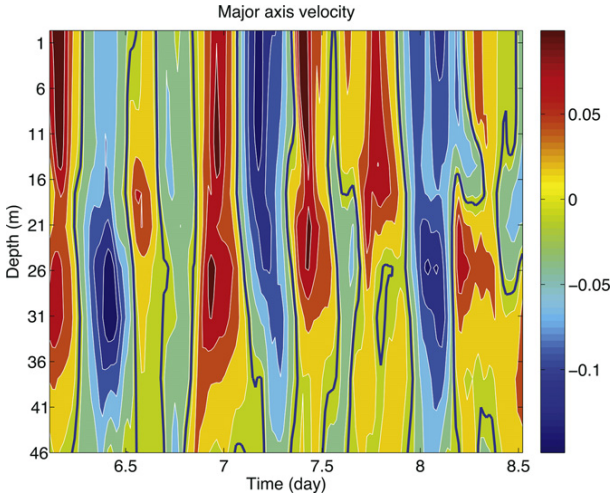

Fig. 8. Three-day window of the detrended velocity ($m\,s^{-1}$) along the major axis of the tidal ellipse centered at the full moon of model month January. Blue thick line is the zero contour. (For interpretation of the references to colour in this figure legend, the reader is referred to the web version of the article.)

moon (Fig. 9d). These results also suggest that the fate of particles according to this metric was mostly independent of the depth of release, although highest percent retained shallower than 200 m were obtained for releases at 40 m (Fig. 9a and b), and 35 m (Fig. 9c). It also suggests that percent within 200 m may vary with changes in diffusivities in the environment.

3.2.2.2. Dispersion characteristics. The absolute dispersion D was calculated for the above-mentioned experiments and for each depth of release. The three-dimensional dispersion was compared between the highest and lowest percentage level for each experiment. The analysis showed that the three-dimensional dispersion was mostly controlled by the vertical component of the dispersion (not shown). The vertical dispersion for each depth of release for 7 January and 9 January showed greater dispersal on the full moon (7 January) than 2 days after the full moon (9 January) (Fig. 10). This correlation between depth of residence and dispersal distances holds for all the release experiments showing that higher percentage of residence less than 200 m depth was correlated with a limited vertical dispersion. The dispersion diagrams also showed more oscillations in the case of limited dispersion on 9 January. Such a pattern is revealing of re-circulating motions that contribute to limited dispersal (Veneziani et al., 2004).

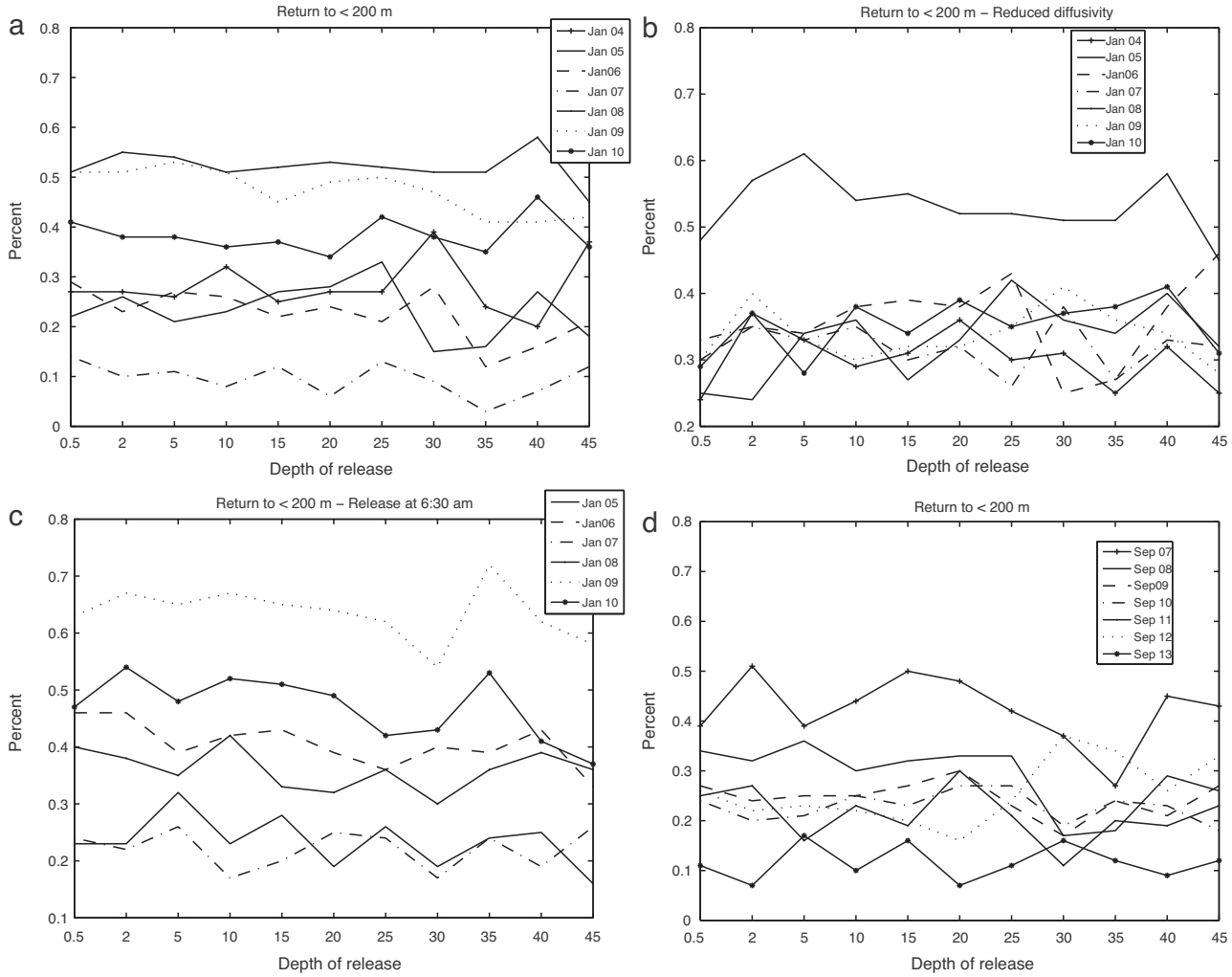

Fig. 9. Percent versus depth (m) of released particles that were found less than 200 m deep within 8 days for different scenarios. Particles were released every day at the same time for 7 days during the week of the full moon (7 January). (a) Release at dusk using the 300 $m^{-2}\,s^{-1}$ diffusivity. (b) Same as (a) using 50 $m^{-2}\,s^{-1}$ diffusivity. (c) Release a dawn using same diffusivity as (a). (d) Release in September at dusk.

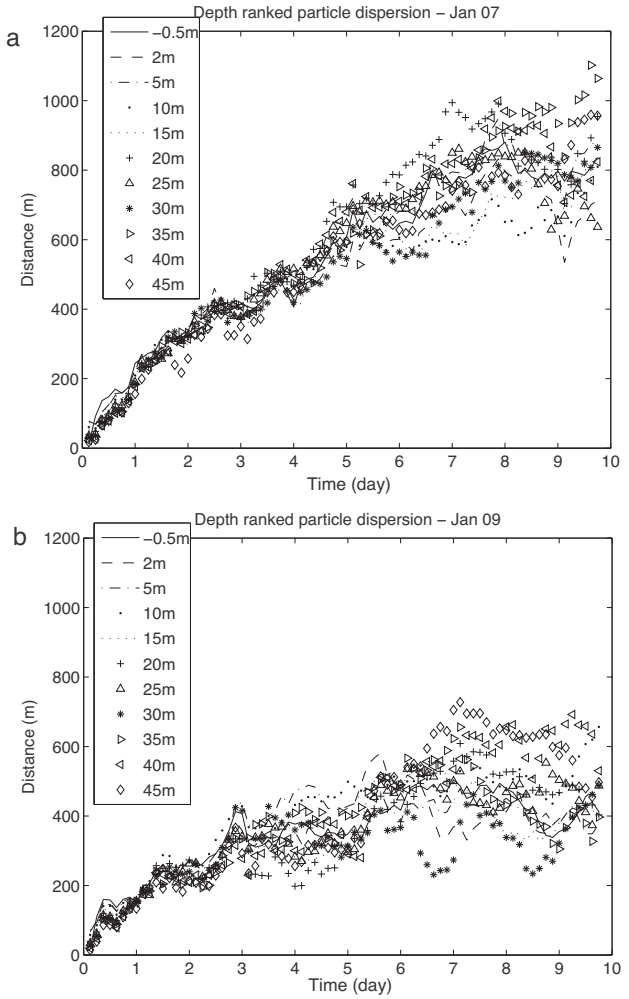

Fig. 10. Absolute vertical dispersion of particle released in January at dusk with 300 m^{-2} s^{-1} diffusivity (a) the day of the full moon (7 January) and (b) 2 days after the full moon (9 January). The symbol corresponds to the depth of release.

3.2.2.3. Trajectories and mesoscale events. Trajectories for two of the release experiments in model month January, one day before and after the full moon showed that in both cases early trajectories were clustered along the shelf edge with more retention on the shelf for the later release (Fig. 11). In December (Fig. 11a and b) particles drifted along the shelf edge and slope and also toward the upper shelf or along the shelf in a more dispersive way than in January (Fig. 11c and d) and February (Fig. 11e and f). In December, the number of particles ending in less than 200 m was particularly high (68%) because particles were entrained toward the shallow shelf by the cyclonic eddy flow. In contrast, the number of particles retained on the shelf in February was very low (~2%) because particles remained in deep water, although they were first clustered along the shelf edge (Fig. 11f). From a three-dimensional perspective, in January, most of the virtual particles followed the shelf slope down then ascended back to the edge of the shelf slope within their 8–10 day journey (Fig. 12).

3.2.3. Physics of the vicinity of the spawning site

3.2.3.1. Tide driven flow direction and energy at spawning time. Assuming that spawning occurs at dusk (Shapiro et al., 1993), results from the NAP flow analysis over the four spawning windows studied (see Section 3.2.1) consistently showed that spawning would occur close to slack tide with the tidal flow in the subsequent hours transporting at first eggs toward the shelf. At this location the tidal flow was always cross isobath, independent of the tide phase. Interestingly, spawning occurred close to the minimum of the tide kinetic energy on the decreasing side of the monthly kinetic energy cycle (Fig. 13), but not at its minimum. This behavior was also observed by Nemeth et al. (2007) in St. Thomas and by Nemeth et al. (2008) at three separate *E. guttatus* spawning sites in the Eastern Caribbean. This may ensure currents strong enough to move the propagules away from the spawning site but with reduced turbulence to reduce patch diffusion.

3.2.3.2. Flow dynamics. The looping trajectories from the spawning site back to its vicinity was coupled with first a downward motion around 65.15°W and then an upward lift east of the latter around 65.05°W (Fig. 12c). The flow at 35 m was similar to the surface westward flow (Fig. 14a) and the flow field at the bottom exhibited currents in different directions and of slower speed that appeared to be constrained by the bottom topography (Fig. 14b). This could induce particles, initially transported toward the shelf, to encounter bottom flow at shallower depths and be transported back to the shelf break in the first 6 h or less and minimize on-shelf transport. South of the eastern-most point of St. Thomas (at 65.15°W) the current flows southward and down the shelf drop-off (Fig. 15a), suggesting downwelling in this region as the density decreases before and at the time of spawning on model day 7 January. Further east (65.05°W) and 8–10 days later, upwelling was present as shown by the increase of density (Fig. 15b).

Finally the passage from the downwelling region to the upwelling region occurred through the presence of a boundary current that flowed eastward along the shelf slope (Fig. 16a). An eastward flow branched from 60 m at the shelf break and extended down to more than 1000 m for the model month of January (Fig. 16b). This flow has been observed by gliders (http://asl.whoi.edu) in January 2008 in the passage between St. Thomas and St. Croix (Fig. 16c).

4. Discussion

4.1. Mean flow at the Red Hind Bank

The flow characteristics at the Red Hind Bank revealed that the mean flow is both vertically sheared and veers to the south in the last 5–10 m above the bottom. The model circulation confirmed the baroclinicity of the flow by showing topography constrained bottom flow, on the shelf, directed to the south, west of the *Epinephelus guttatus* spawning site. This three dimensional structure of the flow suggests that virtual particles first entrained at the spawning site at 300 m in from the shelf edge are pushed into the southward flowing current at the bottom, transporting them to the shelf edge, and this mechanism is supported by the observations of offshore transport (Colin and Bell, 1991; Heyman et al., 2005; Storlazzi et al., 2006). Spawning of *E. guttatus* is believed to occur a few meters above the bottom (Nemeth et al., 2007) and this is where the currents are the weakest (Fig. 5). Particles released close to the bottom can be transported directly to the shelf-break. However, if the buoyant eggs ascend higher in the water column, the initial onshore transport can bring them to the level of the southward flow (Fig. 14b). In any event, the southward transport appears to be independent of the depth of spawning as shown by the model particle trajectories (Figs. 9 and 10).

4.2. Incoherent tide influence

Our observations and model simulations showed that time of spawning was synchronized with on-shore tidal currents, which

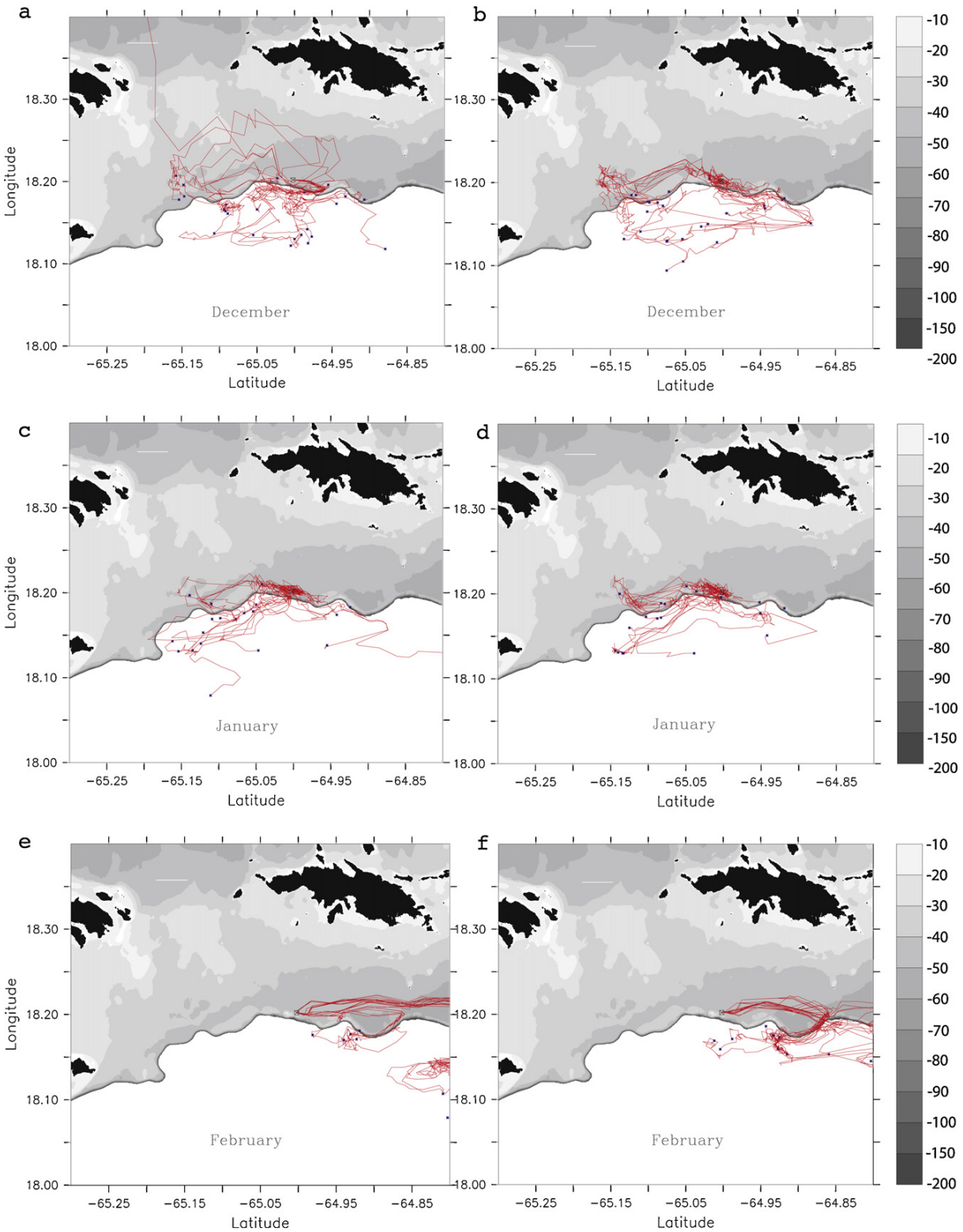

Fig. 11. Particle trajectories for model month December (a and b), January (c and d), and February (e and f). Particles were released 1 day before (left panels) and one day after (right panels) the full moon. Shades of gray show the bathymetry contours every 10 m to −200 m. Black shows land and white areas south of the shelf range from −200 to −4000 m.

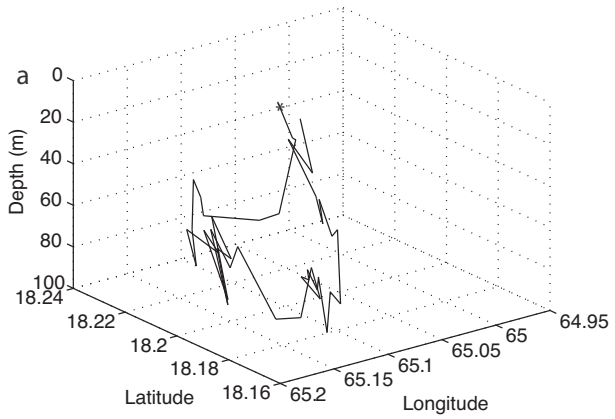

Fig. 12. Three-dimensional looping trajectory plotted every 6 h. The star shows the release location.

contradicted previous observations that spawning was synchronized with the outgoing tide, favoring the transport of fertilized eggs offshore (Colin and Bell, 1991; Heyman et al., 2005; Storlazzi et al., 2006). However, our results could be explained by the local oceanography of the shelf edge at the Red Hind Bank as explained in Section 4.2.

4.3. Timing and trajectories

Model trajectories showed that best return success was for particles released between one and 3 days after the full moon during the month of spawning. During non spawning months, our model showed that the level of return was lower but that the release day leading to best return success could be variable and before the full moon. Interestingly, the 3-day time series in Fig. 5 shows that the flow at the spawning site is weaker close to the bottom than in the middle of the water column in January and February, which fall during the dry season. The observations on flow patterns during the spawning period suggest that a slower current close to the bottom may be one factor determining the timing of spawning. Based on our model simulation of particles, this vertical flow structure seems to favor a better return success, which seems to correspond to the peak of percent return obtained for 35 and 40 m deep releases (Fig. 9). Although information is limited on the vertical distribution patterns of coral reef fishes, serranid larvae, in general, are found mostly at 25–50 m depth (Cha et al., 1994). Taxon-specific information is limited to the small non-commercial *Serranus* spp., which are most abundant at 30–60 m depth (Cowen, 2002).

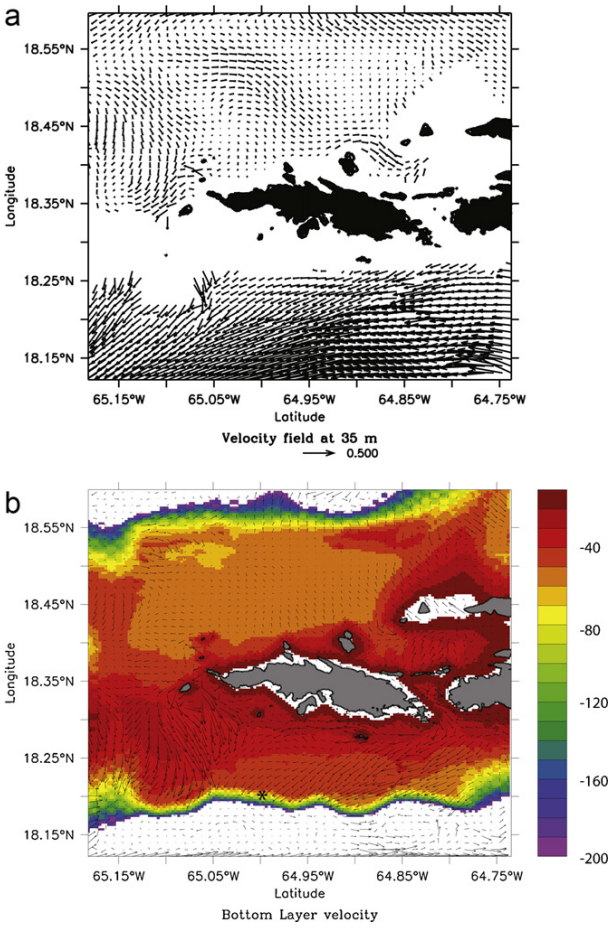

Fig. 14. (a) Model flow field at 35 m deep. (b) Model bottom layer flow field. The layer follows the topography therefore vectors south of the shelf break show the speed at 500 m for the latter. Colors show depth contours. The star shows the spawning aggregation site.

In the model simulation the extent of the particle trajectories that are found less than 200 m depth within 8–10 days is in the range of the adult habitat as described by Nemeth et al. (2008).

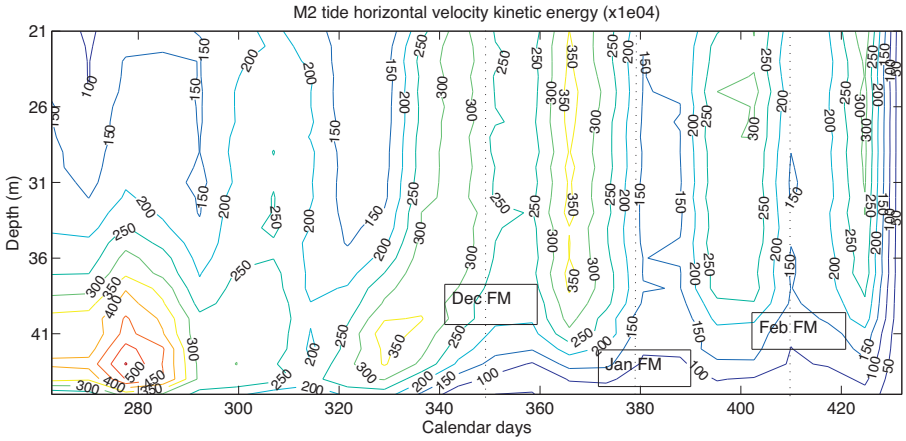

Fig. 13. M2 tide horizontal velocity kinetic energy ($cm^2\ s^{-2}$) in depth and time space for periods P2. Dotted line shows the full moon.

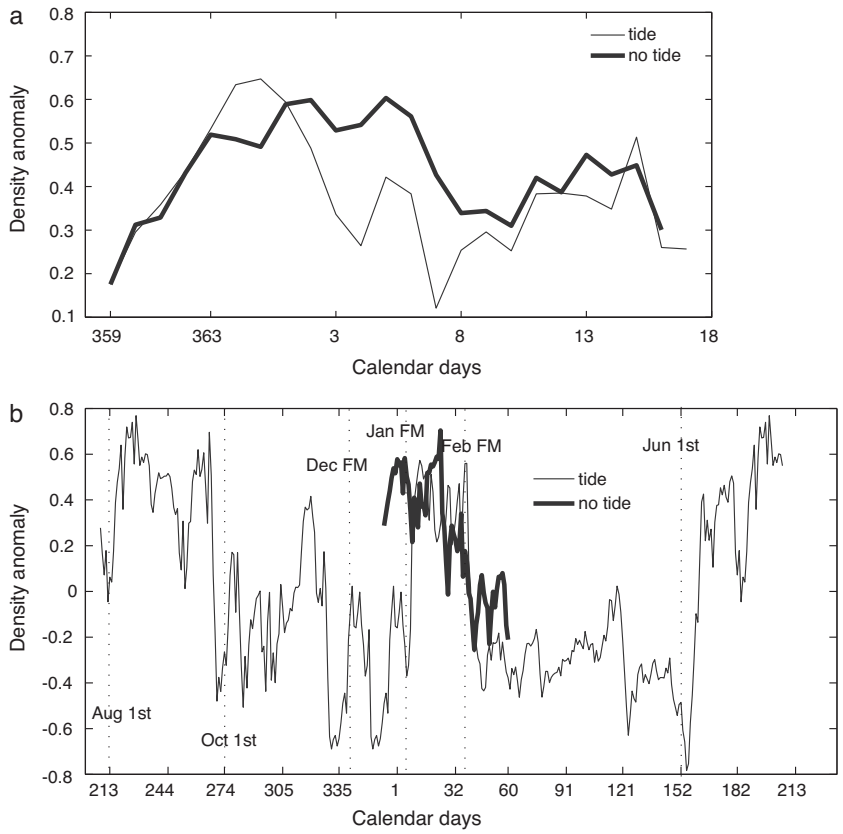

Fig. 15. (a) Model month December–January time series of density anomaly (kg m^{-3}) at the shelf break at 65.15°W. (b) One year time series of the density anomaly at the shelf break, further east at 65.05°W. Thick line shows the density anomaly when the model is run without tide for January and February. Dotted lines show one specific day of a month and the full moons in December 2003 and, January and February 2004.

Moreover, the deep chlorophyll maximum is found between 40 and 200 m in the north-eastern Caribbean Sea (Corredor and Morell, 2001; Smith et al., 2010), which suggests that the particles (and larvae) transported to those depths would encounter more plankton food sources than elsewhere offshore (Cowen, 2002). This enriched plankton layer could constitute a food supply for newly hatched grouper larvae which need to begin feeding once their yolk is absorbed about three to 4 days after fertilization and about 2–3 mm length (Katajima et al., 1992; Colin et al., 1997; Leis and McCormick, 2002; Martínez-Lagos and Gracia-Lopez, 2009). Eight–10 days into their journey, virtual particles were transported back to the edge of the shelf, a scenario, which provides a mechanism that can contribute to retention of grouper larvae. In general, tropical reef fishes have more highly developed fins and sensory organs and are strong swimmers at a relatively small size (Leis and McCormick, 2002). Grouper larvae in particular develop swim bladders about 12 d post hatch and undergo post-flexion stage around day 17, two developmental milestones that enhance buoyancy and swimming capabilities, respectively (Powell and Tucker, 1982; Colin and Koenig, 1996). The average pelagic larval duration for the congeneric Nassau grouper (*E. striatus*) is 41.6 d. Although there is no current knowledge about *E. guttatus* settlement patterns, Colin et al. (1997) found a significant relationship between settlement pulses of larval *E. striatus* and observed spawning in an aggregation in the Bahamas, suggesting that coupling of spawning and subsequent local recruitment may exist in group-spawning Serranidae.

Results of model flow dynamics suggests that tide plays a role in the timing of spawning so that downwelling and upwelling at different locations along the shelf follow a lag pattern (Fig. 15). The year-long time series of the density anomaly variations (Fig. 15b) was in very good agreement with the time series of the vertical distribution of chlorophyll *a* at the CaTS station located southwest of Puerto-Rico and west of St. Thomas (Corredor and Morell, 2001 Plate 1b). In this region, chlorophyll lies at the top of the pycnocline. The chlorophyll maximum layer shoals from June to September to about 40 m depth, followed by some variations in the strength of the upwelling between 75 and 100 m in December and January, followed by a downwelling onward until next June. The downwelling observed during this period was due to the erosion of the pycnocline by the strong trade winds (Corredor and Morell, 2001). In absence of tide, the variations of the density anomaly are different from the ones with tide (Fig. 15b). It suggests that the tide contributed to some of the regular oscillations seen in the density anomaly, controlling the timing of upwelling and downwelling.

The effect of tide was tested on the return success of the virtual particles. Without tide, the number of particles returning to less than 200 m decreased by up to half of those found when the tidal effect was present. The synchronicity between upwelling at the shelf break and the length of the drifting journey appears to be critical for the return success and is driven by the coupling between the wind, which controls the seasonal changes of the depth of the chlorophyll maximum and of the mixed layer (Corredor and Morell, 2001) and the tide induced vertical movements at the shelf break (Fig. 15).

4.4. Effect of sub-mesoscale and mesoscale flow

The presence of a sub-mesoscale cyclonic eddy in December south of the shelf of St. Thomas contributed to the shoreward transport of particles (Fig. 11a and b), although some of the particles

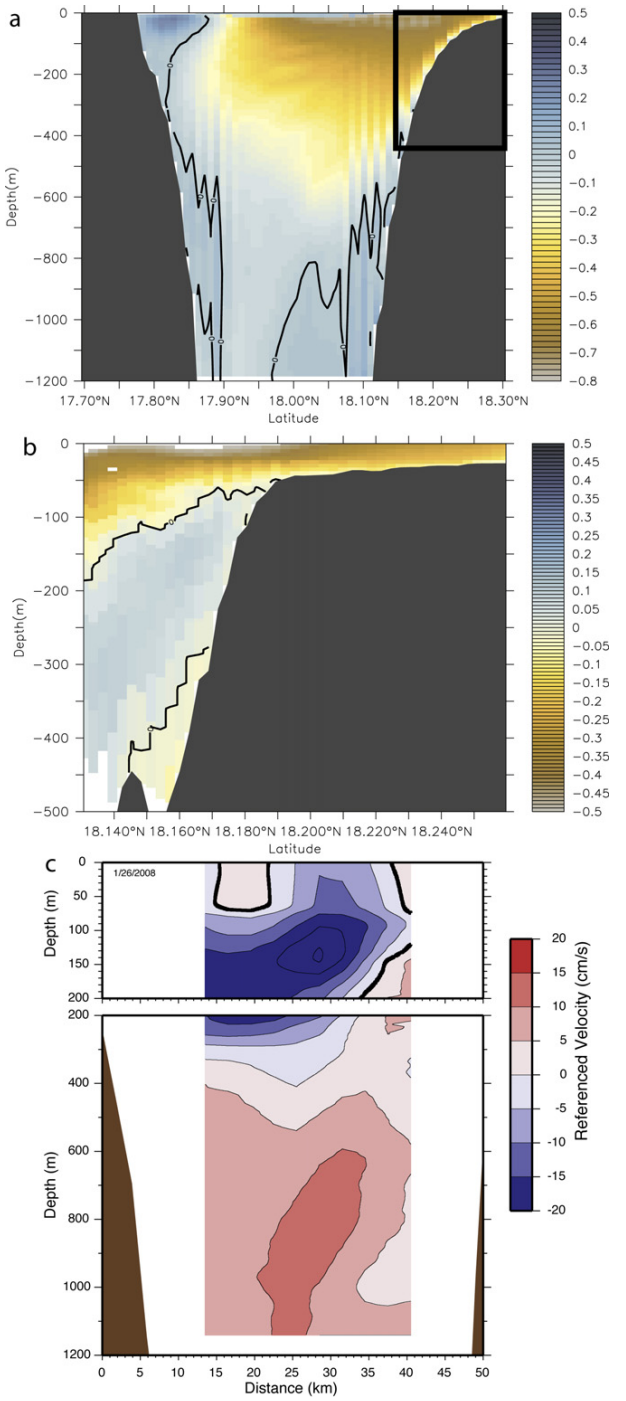

Fig. 16. Meridional section across the shelf at 64.8°W (a) in the 2 km horizontal resolution first child model. The black square shows the zoom of the section in (b) upper 500 m in the 670 m horizontal resolution second child model. (c) Same section observed by gliders in January 2008 (http://asl.whoi.edu). Colour bars show the current velocity and thick black lines the zero contour.

reached the shelf edge. In February, the presence of the eastward current, associated to a change in mesoscale flow (not shown) at the shelf break contributed to transport particles eastward, though most of them returned westward toward the spawning location (Fig. 11e and f). These results suggest that the flow circulation around the spawning site, below the surface, is relatively resilient to changes in direction of the upper flow, and thus to the effects of eddies. Indeed, when virtual particles were released from another location just north of the actual Red Hind Bank spawning site, this produced very similar dispersal trajectories as the ones from the actual site (not shown). Thus it appears that transport history of released particles is not influenced by a particular spawning location, rather the choice of a spawning location may be due to some biological requirement, e.g., fertilization success between gametes or complex habitats, which protect spawning adults from predation (Nemeth, 2009).

This result is similar to simulation studies conducted by Appeldoorn et al. (1994) who found similar dispersal patterns from spawning and nearby non-spawning sites. In our study, bottom currents also bring particles to the shelf edge where they would be driven by the same dynamics. In other locations, cyclonic eddies, gyres and tidal fronts have been shown to affect large-scale current patterns or induce reverse flows that influence larval dispersal and subsequent patterns of settlement (Kingsford and Finn, 1997; Heyman and Kjerfve, 2008). Therefore, the choice of the general vicinity of a spawning site could be guided by the regional flow pattern over the duration of the pre-competency period, while the choice of the specific location in that region would be guided by other factors that have not been yet elucidated, which could be biological in nature.

4.5. Modeling aspects and limitations

The climatological simulation in this study has been used to identify the role of the oceanography of the northeastern Caribbean Sea in the genetic break of the population of coral *Acropora palmata* between the eastern and western Caribbean Sea (Baums et al., 2006). The energetics and dynamics, and their seasonality simulated by the model were shown to be similar to observations (Chérubin and Richardson, 2007). Although the times series obtained at the NAP location in the model is relatively short compared to the observations, the main characteristics of the observed flow are reproduced by the model. Nonetheless, large differences of the mean velocity are present, in particular at the surface and the tide explained variance is not as large as in the observations because of the short model time-series that was used for this study. The critical effect of the tide in the model dynamics is shown by the agreement between the tidal flow characteristics on the shelf. These local discrepancies are mostly explained by the horizontal and vertical resolution of the model, which introduce a smoother topography and a coarser resolution close to the bottom.

Differences in the mean flow speed and direction emanate from the intrinsic smoothed variability carried by the forcing and ocean climatologies, although the main seasonal variability in the wind and the surface salinity is present. A direct comparison between flow events is therefore impossible between a given year and the climatological simulation. Though, as confirmed by previous studies, the dynamical features that are present in the climatological simulation are realistic.

The transport of neutrally buoyant particles is not supported by any direct observations. However all the processes that contribute to the feedback loop were validated by oceanographic data. The direct observation of actual larval trajectories is currently almost impossible to observe with existing technology.

The month of January has been observed as the peak spawning month for *E. guttatus* in the USVI (Nemeth et al., 2008). Moreover, the timing of spawning seems to be consistent within the eastern Caribbean relative to the lunar phase (i.e. spawning before full moon), but this pattern seems to shift to spawning after the full moon in western Puerto Rico (Sadovy et al., 1994; Nemeth et al., 2008). Similar patterns seem to occur for aggregating species which spawn around the large island of Cuba (Claro and Lindeman, 2003).

Although the simulations show higher percents of return for this month, differences with other months and other spawning times are not extremely different. They appear to be more subtle, which could be a result from model inaccuracies but could also reflect the ecological processes driving the precise timing of spawning to be tuned to very specific physical cues, such as the timing of the downwelling and upwelling cycle at the shelf break, which confer a slight advantage to larval survival and retention. Since larval mortality is estimated to be greater than 99%, small advantages to survival may have a relatively large influence on the magnitude of larvae settlement (Jones, 1991). Although tide is thought to play a role in the initial dispersion, it appears that reduced tide driven energy periods are preferred (Fig. 13) and that the regional effect of tides on vertical movement at the shelf break is relevant to particle transport feedback loop.

5. Conclusions

Results from this study suggest that some level of retention may exist for *Epinephelus guttatus* eggs and larvae produced at the Red Hind Bank spawning aggregation site. More sophisticated biophysical models which incorporate larval behavior (swimming and vertical distribution) and vital rates (growth, development and survival) are needed for a more complete understanding of larval distribution patterns and retention mechanisms (Cowen, 2002). When examining the applicability of our results to various competing hypotheses, we found our model outputs to be consistent with several larval survival hypotheses in the pelagic environment (Johannes, 1978). As suggested by Nemeth et al. (2008), there may be overlap between the dispersal of larvae and adult home range. This study found that particles were transported away from the reef and this is consistent with the predator avoidance hypothesis for tropical fish eggs (Johannes, 1978), although particles were transported toward the shelf in the first hours (bringing them close to the bottom flow that transported them back to the shelf break). Remaining close to the reef reduces the chance of eggs and larval survival due to increased predation pressure from planktivores. However since spawning in *E. guttatus* is thought to occur after sunset (Shapiro et al., 1993) more eggs may survive nighttime transport to the shelf edge. Offshore and downward transport allows larvae to come in contact with the chlorophyll maximum, this strategy is consistent with the pelagic survival hypothesis (Johannes, 1978; Cushing, 1972), which assumes that larvae would survive better in a food rich environment (Cowen, 2002). More research on the synchronization of the deep chlorophyll layer with production and transport of eggs and larvae is needed. Moreover, a focus on identifying the vertical larval distribution patterns of the commercially important Epinephelinae, which form spawning aggregations, is warranted and this study provides guidance on potential depth strata where they may be found. The mechanisms that allow for transport away and return to the reef edge is consistent with the egg dispersal and larval retention hypothesis (Johannes, 1978). This hypothesis suggests that larvae return to a suitable habitat that could be within the range of their parents' habitat.

Tide acts as a mechanism of retention that maximizes the likeliness that particles will be transported away from the reef to where food is available and back to their area of release. The choice of the spawning location seems to depend on the resilience of the above scenario of transport to mesoscale flow changes and also to the systematic southward transport regardless of the depth of spawning. Nonetheless, eddies could enhance recruitment events on the shallow part of the reef and beyond the parents' habitat, or unusual currents could potentially reduce retention by transporting eggs away from the region of returning flow. Besides the good agreement and consistency of the circulation model with the observations, using these results to describe propagule transport in reality should be interpreted with caution because the Lagrangian life history of the eggs and larvae remain observationally unknown in the environment.

Acknowledgments

The authors are thankful to personnel of University of the Virgin Islands, Kevin Brown for providing the Aquadopp profiler data; Tyler Smith and Elizabeth Kadison for fruitful discussions. The authors greatly appreciate discussions with Claire Paris at the University of Miami. The authors are also thankful to Dave and Paula Fratantoni for providing the gliders' data. This study was funded by U. S. Geological Survey State Partnership Program cooperative agreement (#07ERAG0078) and supported by subcontract No. EPSCOR 2006-04 funded by NSF grant to UVI No. EPS-0346483. This is contribution #59 from the Center for Marine and Environmental Studies at the University of the Virgin Islands. Any opinions, findings, conclusions, or recommendations expressed in the material are those of the authors and do not necessarily reflect the views of NSF and USGS.

References

Appeldoorn, R.S., Hensley, D.A., Shapiro, D.Y., Kioroglou, S., Sanderson, B.G., 1994. Egg dispersal in a Caribbean coral reef fish, *Thalassoma bifasciatum*. II. Dispersal off the reef platform. Bull Mar Sci 54, 271–280.

Armstrong, R.A., Singh, H., Torres, J., Nemeth, R.S., Can, A., Roman, C., Eustice, R., Riggs, L., Garcia-Moliner, G., 2006. Characterizing the deep insular shelf coral reef habitat of the Hind Bank marine conservation district (US Virgin Islands) using the Seabed autonomous underwater vehicle. Cont Shelf Res 26, 194–205.

Barlow, G.W., 1981. Patterns of parental investment, dispersal and size among coral reef fishes. Environ Biol Fishes 6, 65–85.

Baums, I., Paris, C.B., Chérubin, L.M., 2006. A dynamic filter to larval dispersal in a reef-building coral. Limnol Oceanogr 49 (6), 1969–1981.

Beets, J., Friedlander, A., 1999. Evaluation of a conservation strategy: a spawning aggregation closure for red hind, *Epinephelus guttatus*, in the U.S. Virgin Islands. Environ Biol Fishes 55, 91–98.

Burnett-Herkes, J., 1975. Contribution to the biology of the red hind, *Epinephelus guttatus*, a commercially important serranid fish from the tropical western Atlantic. PhD thesis, University of Miami, Coral Gables, p. 154.

Cha, S.S., McGowan, M.F., Richards, W.J., 1994. Vertical distribution of fish larvae of the Florida Keys, 26 May–5 June 1989. Bull Mar Sci 54, 828–842.

Chérubin, L.M., Richardson, P., 2007. Caribbean current variability and the influence of the Amazon and Orinoco fresh water plumes. Deep-Sea Res. I 54, 1451–1473.

Claro, R., Lindeman, K.C., 2003. Spawning aggregation sites of snapper and grouper species (*Lutjandidae* and *Serranidae*) on the insular shelf of Cuba. Gulf Carib Res 14, 91–106.

Colin, P.L., 1992. Reproduction of the Nassau grouper, *Epinephelus striatus* (Pisces: *Serranidae*) and its relationship to environmental conditions. Environ Biol Fish 34, 357–377.

Colin, P.L., Shapiro, D.Y., Weiler, D., 1987. Aspects of reproduction of two species of groupers, *Epinephelus guttatus* and *E. striatus*, in the West Indies. Bull Mar Sci 40, 220–230.

Colin, P.L., Bell, L.J., 1991. Aspects of spawning of labrid and scarid fishes (Pisces: *Labroidei*) at Enewetak Atoll, Marshall Islands with notes on other families. Environ Biol Fish 31, 229–260.

Colin, P.L., Laroche, W.A., Brothers, E.B., 1997. Ingress and settlement in the Nassau grouper, *Epinephelus striatus* (Pisces: *Serranidae*), with relationship to spawning occurrence. Bull Mar Sci 60, 656–667.

Colin, P.L., Koenig, C.C., 1996. Spines in larval red grouper, *Epinephelus morio*: development and function. Proc Gulf Carib Fish Inst 44, 31–38.

Corredor, J.E., Morell, J.M., 2001. Seasonal variation of physical and biogeochemical features in eastern Caribbean surface water. J Geophys Res 106 (C3), 4517–4525.

Cowen, R.K., 2002. Larval dispersal and retention and consequences for population connectivity. In: Sale, P.F. (Ed.), Coral Reef Fishes: Dynamics and Diversity in a Complex Ecosystem. Academic Press, London, pp. 149–170.

Cowen, R.K., Paris, C.B., Srinivasan, A., 2006. Scaling connectivity in marine populations. Science 311, 522–527.

Cushing, D.H., 1972. The production cycle and the numbers of marine fish. Symp Zool Soc Lond 29, 213–232.

Doherty, P.J., Williams DMcB, Sale, P.F., 1985. The adaptive significance of larval dispersal in coral reef fishes. Environ Biol Fish 12 (2), 81–90.

Domeier, M.L., Colin, P.L., 1997. Tropical reef fish aggregations: defined and reviewed. Bull Mar Sci 60 (3), 698–726.

Egbert, G., Erofeeva, S., 2002. Efficient inverse modeling of barotropic ocean tides. J. Atmos Ocean Tech 19, 183–204.

Gladstone, W., 2007. Selection of a spawning aggregation site by *Chromis hypsilepis* (Pisces: *Pomacentridae*): habitat structure, transport potential, and food availability. Mar Ecol Progr Ser 351, 235–247.

Hensley, D.A., Appeldoorn, R.S., Shapiro, D.Y., Ray, M., Turingen, R.G., 1994. Egg dispersion in a coral reef fish, *Thalassoma bifasciatum*. I. Dispersal over the reef platform. Bull Mar Sci. 54, 256–270.

Heyman, W., Requena, N., 2002. Status of multi-species spawning aggregations in Belize. Punta Gorda, Belize, The Nature Conservancy, pp. 3–27.

Heyman, W.D., Kjerfve, B., Graham, R.T., Rhodes, K.L., Garbutt, L., 2005. Spawning aggregations of *Lujanus cyanopterus* (cuvier) on Belize Barrier Reef over a 6 year period. J Fish Biol 67, 83–101.

Heyman, W.D., Kjerfve, B., 2008. Characterization of transient multi-species reef fish spawning aggregations at Gladden Spit, Belize. Bull Mar Sci 83, 531–551.

Johannes, R.E., 1978. Reproductive strategies in coastal marine fishes in the tropics. Environ Biol Fishes 3, 65–84.

Jones, G.P., 1991. Postrecruitment processes in the ecology of coral reef fish populations: a multifactorial perspective. In: Sale, P.F. (Ed.), The Ecology of Fishes on Coral Reefs. Academic Press, Inc, San Diego, pp. 294–330.

Kadison, E., Nemeth, R., Herzlieb, S., Blondeau, J., 2006. Temporal and spatial dynamics of Lutjanus cyanopterus and L. jocu (Pisces: Lutjanidae) spawning aggregations on a multi-species spawning site in the USVI. Rev Biol Trop 54 (s3), 69–78.

Katajima, C., Takaya, M., Tsukashima, Y., Arakawa, T., 1992. Development of eggs, larvae and juveniles of the grouper (*Epinephelus septemfasciatus*) reared in the laboratory. Jap J Ich 38 (1), 47–55.

Kingsford, M., Finn, M., 1997. The influence of phase of the moon and physical processes on the input of presettlement fishes to coral reefs. J Fish Biol 51, 176–205.

Leffler, K.E., Jay, D.A., 2009. Enhancing tidal harmonic analysis: Robust (hybrid L1/L2) solutions. Con Shelf Res 29, 78–88.

Leis, J.M., McCormick, M.I., 2002. The biology, behavior, and ecology of the pelagic larval stage of coral reef fishes. In: Sale, P.F. (Ed.), Coral Reef Fishes: Dynamics and Diversity in a Complex Ecosystem. Academic Press, Inc, Boston, pp. 171–199.

Lobel, P. Diel, 1978. lunar and seasonal periodicity in the reproductive behavior of the pomacanthid fish, Centropyge potteri, and some other reef fishes in Hawaii. Pac. Sci. 32, 193–207.

Luckhurst, B.E., 1998. Site fidelity and return migration of tagged red hinds (*Epinephelus guttatus*) to a spawning aggregation site in Bermuda. Proc 50th Gulf Carib Fish Inst 50, 750–763.

Luckhurst, B.E., 2010. Observations of a black grouper (*Mycteroperca bonaci*) spawning aggregation in Bermuda. Gulf Carib Res 22, 43–49.

Martínez-Lagos, R., Gracia-Lopez, V., 2009. Morphological development and growth patterns of the leopard grouper (*Mycteroperca rosacea*) during larval development. Agric Res 41 (1), 120–128.

Moyer, J.T., 1989. Reef channels as spawning sites for fishes on the Shiraho coral reef, Ishigaki Island, Japan. Japan J Ichthyol 36, 371–375.

Nemeth, R.S., 2005. Population characteristics of a recovering US Virgin Islands red hind spawning aggregation following protection. Mar Ecol Prog Ser 286, 81–97.

Nemeth, R.S., Kadison, E., Herzlieb, S., Blondeau, J., Whiteman, E., 2006. Status of a Yellowfin Grouper (*Mycteroperca venenosa*) Spawning Aggregation in the US Virgin Islands with Notes on Other Species, vol. 57 , Proc 57th Gulf Carib Fish Inst. St. Petersburg, FL, pp. 543–558.

Nemeth, R.S., Blondeau, J., Herzlieb, S., Kadison, E., 2007. Spatial and temporal patterns of movement and migration at spawning aggregations of red hind, *Epinephelus guttatus*, in the U.S. Virgin Islands. Environ Biol Fishes 78, 365–381.

Nemeth, R.S., Kadison, E., Blondeau, J.E., Idrisi, N., Watlington, R., Brown, K., Smith, T., Carr, L., 2008. Regional coupling of red hind spawning aggregations to oceanographic processes in the eastern Caribbean. In Grober-Dunsmore, R., Keller, B.D., editors. Caribbean connectivity: Implications for marine protected area management. Proc 59th Gulf Carib Fish Inst., 2006; Marine Sanctuaries Conservation Series NMSP-08-07, pp. 170–183.

Nemeth, R.S., 2009. Dynamics of reef fish and decapod crustacean spawning aggregations: underlying mechanisms, habitat linkages and trophic interactions. Ecological interactions among tropical coastal ecosystems. I. Nagelkerken, Springer, pp. 73–134.

Okubo, A., 1971. Oceanic diffusion diagrams. Deep-Sea Res 18, 789–802.

Paris, C.B., Cowen, R.K., 2004. Direct evidence of a biophysical retention mechanism for coral reef fish larvae. Limnol Oceanogr 49, 1964–1979.

Paris, C.B., Cherubin, L.M., Cowen, R.K., 2007. Surfing, spinning, or diving from reef to reef: effects on population connectivity. Mar Ecol Prog Ser 347, 285–300.

Pawlowicz, R., Beardsley, B., Lentz, S., 2002. Classical tidal harmonic analysis including error estimates in MATLAB using T-TIDE. Comput Geosci 28, 929–937.

Powell, A.B., Tucker, J.W., 1982. Egg and larval development of laboratory-reared Nassau grouper, *Epinephelus striatus* (Pisces, *Serranidae*). Bull Mar Sci 50 (1), 171–185.

Richards, W.J., Baldwin, C.C., Ropke, A., 2006. Serranidae: sea basses. In: Richards, W.J. (Ed.), Early stages of Atlantic fishes: an identification guide for western central North Atlantic, vol. 1. CRC Press, Boca Raton, FL, pp. 1225–1331.

Richardson, P.L., 2005. Caribbean Current and eddies as observed by surface drifters. Deep-Sea Res II 52, 429–463.

Robertson, D.R., Hoffman, S.G., 1977. The roles of female mate choice and predation in the mating systems of some tropical labroid fishes. Z Tierpshychol 45, 298–320.

Robertson, D.R., 1991. The role of adult biology in the timing of spawning of tropical reef fishes. In: Sale, P.F. (Ed.), The Ecology of Fishes on Coral Reefs. Academic Press, Inc, San Diego, pp. 356–370.

Ross, R.M., 1983. Annual, semilunar, and diel reproductive rhythms in the Hawaiian labrid *Thalassoma duperrey*. Mar Biol 72, 311–318.

Sadovy, Y., Eklund, A.-M., 1999. Synopsis of biological data on the Nassau grouper, *Epinephelus striatus* (Bloch, 1792), and the Jewfish, *E. itajara* (Lichtenstein, 1822). Seattle, Washington, pp. 1–85.

Sadovy, Y., Rosario, A., Roman, A., 1994. Reproduction in an aggregating grouper, the red hind, *Epinephelus guttatus*. Environ Biol Fishes 41, 269–286.

Sadovy-de-Mitcheson, Y., Cornish, A., Domeier, M., Colin, P.L., Russell, M., Lindeman, K.C., 2008. A global baseline for spawning aggregations of reef fishes. Conserv Biol 22, 1233–1244.

Sala, E., Ballesteros, E., et al., 2001. Rapid decline of Nassau grouper spawning aggregations in Belize: fishery management and conservation needs. Fisheries 26, 23–30.

Shapiro, D.Y., Sadovy, Y., McGehee, M.A., 1993. Size, composition, and spatial structure of the annual spawning aggregation of the red hind, *Epinephelus guttatus* (Pisces: *Serranidae*). Copeia 2, 399–406.

Shchepetkin, A.F., McWilliams, J.C., 2004. Regional Ocean Model System: a split-explicit ocean model with a free-surface and topography-following vertical coordinate. Ocean Model 9, 347–404.

Smith, T.B., Blondeau, J., Nemeth, R.S., Calnan, J.M., Kadison, E., Gass, J., 2010. Benthic structure and cryptic mortality in a Caribbean mesophotic coral reef bank system, the Hind Bank Marine Conservation District, U.S. Virgin Islands. Coral Reefs 29, 289–308.

Starr, R.M., Sala, E., Ballesteros, E., Zabala, M., 2007. Spatial dynamics of the Nassau grouper *Epinephelus striatus* in a Caribbean atoll. Mar Ecol Progr Ser 343, 239–249.

Storlazzi, C.D., Brown, E.K., Field, M.E., 2006. The application of acoustic Doppler current profilers to measure the timing and patterns of coral larval dispersal. Coral Reefs 25 (3), 369–381.

van Aken, H.M., van Haren, H., M.Maas, L.R., 2007. The high-resolution vertical structure of internal tides and near inertial waves measured with ADCP over the continental slope in the Bay of Biscay. Deep-Sea Res I 54, 533–556.

Veneziani, M., Griffa, A., Reynolds, A.M., Mariano, A.J., 2004. Oceanic turbulence and stochastic models from subsurface Lagrangian data for the Northwest Atlantic Ocean. J Phys Oceanog 34 (8), 1884–1906.

Whaylen, L., Pattengill-Semmens, C.V., Semmens, B.X., Bush, P.G., Boardman, M.R., 2004. Observations of a Nassau grouper (*Epinephelus striatus*) spawning aggregation site in Little Cayman, including multi-species spawning information. Environ Biol Fishes 70, 305–313.